バイオサイエンス研究科　博士論文要旨

所　属 (主指導教官)	生体高分子構造学講座（箱嶋敏雄 教授）		
氏　名	岸　忠明	提　出	平成 13 年 1 月 9 日
題　目	Structural and Biochemical Studies of Neuropsin, a Serine Protease Expressed in the Limbic System of Mouse Brain, and Its Specific Inhibitor (マウス脳内プロテアーゼneuropsinとその特異的インヒビターの構造学的、生化学的研究)		

要旨

Extracellular serine protease neuropsin is expressed in the forebrain limbic area of adult brain and is implicated in synaptic plasticity. In the present study, (1) I characterized a crystal structure of neuropsin and (2) I identified a possible endogenous inhibitor specific for neuropsin *in vivo*.

First, recombinant neuropsin was produced using a baculovirus expression system and was purified. Two crystal forms were obtained by a hanging-drop vapor-diffusion method with polyethylene glycol (PEG). Crystal form I belongs to triclinic space group *P1* with unit cell dimensions a = 97.16 Å, b = 97.12 Å, c = 46.75 Å and α = 99.17°, β = 99.77°, γ = 117.35°. There were six molecules in the crystallographic asymmetric unit. Crystal form II also belongs to triclinic space group *P1* but has unit cell dimensions a = 38.40 Å, b = 55.16 Å, c = 65.37 Å and α = 95.38°, β = 89.98°, γ = 110.46°. Intensity data to 3.1 Å resolution for form I and to 2.1 Å for form II were collected. The 2.1-Å crystal structure of neuropsin provides the three-dimensional view of one of the serine proteases highly expressed in the nervous system, and reveals a serine protease fold that exhibits chimeric features between trypsin and nerve growth factor (NGF)-γ, a member of the kallikrein family. Neuropsin possesses an *N*-glycosylated "kallikrein loop" but forms six disulfide bonds corresponding to those of trypsin. The ordered kallikrein loop projects proline toward the active site to restrict smaller residues or proline at the P2 position of substrates. The loop F, which participates in forming the S3/S4 sites, is similar to trypsin rather than NGF-γ. The unique conformations of the loops G and H form an S1 pocket specific for both arginine and lysine. These characteristic loop structures forming the substrate-binding site suggest the novel substrate specificity.

Second, a neuropsin inhibitor was detected as an SDS-stable complex with recombinant neuropsin in extracts of the hippocampus and cerebral cortex in adult mouse. After the purification (a 3.3 x 10^2-fold purification and a yield of 1.5%), peptide sequences were determined by amino acid sequencing and mass spectrometry, revealing that endogenous serine proteinase inhibitor 3 (SPI3) contributed to the formation of the SDS-stable complex with recombinant neuropsin. Addition of the recombinant SPI3, prepared with a *Pichia pastoris* expression system, to recombinant neuropsin resulted in an SDS-stable complex and the complex formation followed bimolecular kinetics with an association rate constant (k_{ass}) of 3.4 ± 0.22 x 10^6 $M^{-1}s^{-1}$ and a dissociation constant (K_i) of 0.8 nM, showing that SPI3 was a slow, tight binding inhibitor of neuropsin. Furthermore, *in situ* hybridization histochemistry showed that SPI3 mRNA was expressed in the limbic system, with the most intense hybridization signals in pyramidal neurons in the CA1-3 subfields of the hippocampus, as was neuropsin mRNA. The finding indicates that SPI3 may inactivate neuropsin to control the activity level of neuropsin in adult brain.

These structural and biochemical studies of neuropsin and its specific inhibitor provide the clues to elucidate the mechanism of memory formation and to drug-design in treatment of pathological conditions such as epilepsy.

Structural and Biological Studies of Neuropsin, a Serine Protease Expressed in the Limibic System of Mouse Brain, and Its Specific Inhibitor
(マウス脳内プロテアーゼneuropsinとその特異的インヒビターの構造学的、生化学的研究)

岸　忠明
奈良先端科学技術大学院大学
バイオサイエンス研究科　生体高分子構造学講座
(箱嶋　敏雄　教授)

平成１３年　１月　９日提出

CONTENTS

ABBREVIATIONS

AcNPV	*Autographa californica* nuclear polyhedrosis virus
AL	amygdaloid complex
Ao	anterior olfactory nuclei
AP	alkaline phosphatase
API	*Achromobacter lyticus* protease I
BCA	bicinchoninic acid
Boc	*t*-butyloxycarbonyl
bp	base pair
BPB	bromophenol blue
BSA	bovine serum albumin
C-terminal	carboxyl terminal
C-terminus	carboxyl terminus
CA1-3	subfields CA1-3 of Ammon's horn
CBB	coomassie brilliant blue
Cc	correlation coefficient
cc	corpus callosum
cDNA	complementary DNA
Cg	cingulate cortex
cp	choroid plexus in lateral ventricle
DG	dentate gyrus
DTT	dithiothreitol
D.W.	distilled water
E-LTP	early-phase long-term potentiation
EBI	The European Bioinformatics Institute
ECM	extracellular matrix
EDTA	ethylenediamine-N,N,N',N'-tetraacetic acid
Ent	entorhinal cortex
Fuc	fucose
FR	frontal cerebral cortex
GlcNAc	*N*-acetylglucosamine
Hb	habenular nucleus
HDB	horizontal diagonal band
HEPES	*N*-2-hydroxyethylpiperazine-*N*-ethanesulfonic acid
HPLC	high pressure liquid chromatography

Hy	hypothalamus
I-V	layers of the frontal cortex
IgG	immunoglobulin G
k_{ass}	association constant
k_{cat}	catalytic constant
K_i	dissociation constant
K_m	the Michaelis-Menten constant
k_{obs}	the apparent first order rate constant
LV	lateral ventricle
mAb	monoclonal antibody
MADLDI-TOF	matrix-assisted laser desorption/ionization time-of-flight
Man	mannose
MCA	4-methylcoumaryl-7-amide
MCS	multiple cloning site
mRNA	messenger RNA
MS	medial septal nucleus
MSP	myelencephalon specific protease
MUG1	murinoglobulin 1
M.W.	molecular weight
N-terminal	amide terminal
NBRF	The National Biomedical Research Foundation
NCBI	The National Center for Biotechnology Information
NGF	nerve growth factor
pAb	polyclonal antibody
PCR	polymerase chain reaction
PDB	The Protein Data Bank
PEG	polyethylene glycol
PI-6	proteinase inhibitor 6
PIR	The Protein Information Resource
PMSF	phenylmethylsulfonyl fluoride
PN-1	protease nexin 1
*p*NA	*p*-nitroanilide
PVDF	polyvinylidene difluoride
R	R-factor
r.m.s.	root mean square
RCSB	The Research Collaboratory for Structural Bioinformatics

SDS	sodium dodecyl sulfate
SDS-PAGE	sodium dodecyl sulfate polyacrylamide gel electrophoresis
SIB	The Swiss Institute of Bioinformatics
SPI3	serine proteinase inhibitor 3
STI	soybean trypsin inhibitor
TBS	Tris-buffered saline
TFA	trifluoroacetic acid
Th	thalamus
tPA	tissue plasminogen activator
Tris	Tris (hydroxymethyl) aminomethane
Triton X-100	*t*-octylphenoxy-polyethoxyethanol
TTBS	TBS buffer with 0.1% Tween 20
Tween 20	polyoxyethylene (20) sorbitan monolaurate
VDB	vertical diagonal band

SUMMARY

Extracellular serine protease neuropsin is expressed in the forebrain limbic area of adult brain and is implicated in synaptic plasticity. In the present study, (1) I characterized a crystal structure of neuropsin and (2) I identified a possible endogenous inhibitor specific for neuropsin *in vivo*.

First, recombinant neuropsin was produced using a baculovirus expression system and was purified. Two crystal forms were obtained by a hanging-drop vapor-diffusion method with polyethylene glycol (PEG). Crystal form I belongs to triclinic space group *P1* with unit cell dimensions $a = 97.16$ Å, $b = 97.12$ Å, $c = 46.75$ Å and $\alpha = 99.17°$, $\beta = 99.77°$, $\gamma = 117.35°$. There were six molecules in the crystallographic asymmetric unit. Crystal form II also belongs to triclinic space group *P1* but has unit cell dimensions $a = 38.40$ Å, $b = 55.16$ Å, $c = 65.37$ Å and $\alpha = 95.38°$, $\beta = 89.98°$, $\gamma = 110.46°$. Intensity data to 3.1 Å resolution for form I and to 2.1 Å for form II were collected. The 2.1-Å crystal structure of neuropsin provides the three-dimensional view of one of the serine proteases highly expressed in the nervous system, and reveals a serine protease fold that exhibits chimeric features between trypsin and nerve growth factor (NGF)-γ, a member of the kallikrein family. Neuropsin possesses an *N*-glycosylated "kallikrein loop" but forms six disulfide bonds corresponding to those of trypsin. The ordered kallikrein loop projects proline toward the active site to restrict smaller residues or proline at the P2 position of substrates. The loop F, which participates in forming the S3/S4 sites, is similar to trypsin rather than NGF-γ. The unique conformations of the loops G and H form an S1 pocket specific for both arginine and lysine. These characteristic loop structures forming the substrate-binding site suggest the novel substrate specificity.

Second, a neuropsin inhibitor was detected as an SDS-stable complex with recombinant neuropsin in extracts of the hippocampus and cerebral cortex in adult mouse. After the purification (a 3.3 x 10^2-fold purification and a yield of 1.5%), peptide

sequences were determined by amino acid sequencing and mass spectrometry, revealing that endogenous serine proteinase inhibitor 3 (SPI3) contributed to the formation of the SDS-stable complex with recombinant neuropsin. Addition of the recombinant SPI3, prepared with a *Pichia pastoris* expression system, to recombinant neuropsin resulted in an SDS-stable complex and the complex formation followed bimolecular kinetics with an association rate constant (k_{ass}) of $3.4 \pm 0.22 \times 10^6$ $M^{-1}s^{-1}$ and a dissociation constant (K_i) of 0.8 nM, showing that SPI3 was a slow, tight binding inhibitor of neuropsin. Furthermore, *in situ* hybridization histochemistry showed that SPI3 mRNA was expressed in the limbic system, with the most intense hybridization signals in pyramidal neurons in the CA1-3 subfields of the hippocampus, as was neuropsin mRNA. The finding indicates that SPI3 may inactivate neuropsin to control the activity level of neuropsin in adult brain.

These structural and biochemical studies of neuropsin and its specific inhibitor provide the clues to elucidate the mechanism of memory formation and to drug-design in treatment of pathological conditions such as epilepsy.

1. INTRODUCTION

Extracellular proteolysis exerted by secretory serine proteases has been implicated in neural development, plasticity, and degeneration and regeneration in the nervous system (Shiosaka and Yoshida, 2000). Neuropsin is an extracellular serine protease cloned from a mouse hippocampal complementary DNA (cDNA) library (Chen *et al.*, 1995) and has been demonstrated to be engaged in activity-dependent plasticity changes in neurons. Neuropsin messenger RNA (mRNA) and protein levels increased in the hippocampus after kindled-seizures and injection of antibody against neuropsin led to retardation of epilepticus in mice (Okabe *et al.*, 1996; Momota *et al.*, 1998). Furthermore, application of recombinant neuropsin induced an increase in the amplitude of the tetanic-stimulation-induced early-phase long-term potentiation (E-LTP) in the Schaffer collateral pathway of the mouse hippocampus (Komai *et al.*, 2000). It has been estimated that neuropsin involves neural plasticity by means of interactions with specific substrates or inhibitors.

Previous studies have shown that neuropsin has proteolytic activity against the C-terminus of arginine or lysine and exhibits the highest sensitivity to a tripeptide substrate preferred for thrombin (Shimizu *et al.*, 1998). To date, many structures of serine proteases have been determined to clarify the mechanisms of their enzymatic actions and unique specificities. Structural knowledge of neuropsin might show important sites for its enzymatic activity and provide clues for searching its specific substrates which are unknown.

Identification of specific inhibitors for neuropsin is also important to analyze enzymatic activity of neuropsin *in vivo*. Generally, serine proteases are controlled by specific inhibitors as serpins (Potempa *et al.*, 1994) and it is likely that neuropsin are also controlled by its specific inhibitor *in vivo*. To detect when and where a specific inhibitor regulates proteolytic activity of neuropsin in brain might provide clues to the biological activity of neuropsin *in vivo*.

In these studies, neuropsin was crystallized and analyzed its ternary structure. Moreover, serine proteinase inhibitor 3 (SPI3) was identified as a specific inhibitor for neuropsin in the adult mouse brain. Knowledge of these studies provides clues to the biological activity of neuropsin and is also important to design of drugs that might be useful in treatment of pathological conditions such as epilepsy.

2. CRYSTAL STRUCTURE OF NEUROPSIN

2-1. MATERIALS AND METHODS

Protein Expression and Purification

Preproneuropsin was over-expressed using a baculovirus expression system, Baculo Gold Transfection Kit (PharMingen, USA), with high five insect cells. High five insect cells were grown at 27℃ in a TNM-FH medium (Hink, 1970; Table 2-1-1) containing 10% heat-inactivated fetal calf serum (Boehringer Mannheim, Germany) to a density of 7 x 10^6 cells/75-cm^2 tissue culture flask. These cells at a density of 1 x 10^6 cells/ml in serum-free medium (Table 2-1-2), Sf-900II SFM (Life Technologies, Inc., USA), were infected with the recombinant baculovirus containing an *Autographa californica* nuclear polyhedrosis virus (AcNPV) genome, which carries a gene encoding preproneuropsin (Shimizu *et al.*, 1998). The infected cells were cultured for 3.5 days at 27℃. Neuropsin was purified by two column chromatographic steps. The culture medium containing neuropsin was dialyzed against 10 mM *N*-2-Hydroxyethylpiperazine-*N'*-ethanesulfonic acid (HEPES) buffer (pH 7.4) at 4℃ for 4 days. The dialyzed medium was applied onto an anion exchange column, RESOURCE S (bet 6 ml; Amersham Pharmacia Biotech, UK), equilibrated previously with 10 mM HEPES buffer (pH 7.4). Proteins were eluted with an 100 ml linear NaCl gradient from 50 to 250 mM. Fractions containing neuropsin were eluted at ~50 mM NaCl. Then, these fractions were applied onto a Heparin column, HiTrap Heparin (bet 5 ml; Amersham Pharmacia Biotech, UK), equilibrated previously with 10 mM HEPES buffer (pH 7.4). Proteins were eluted with a 90 ml linear NaCl gradient from 200 to 500 mM. Fractions containing neuropsin were eluted at ~ 280 mM NaCl. Approximately 8 mg of purified neuropsin was obtained from a 1.3 litter-culture medium. For crystallization studies, the protein was concentrated to 24.5 mg/ml in a solution containing 5 mM HEPES buffer (pH 7.4) and 100 mM NaCl using a centrifugal concentrator, Centricon10 (Amicon, USA). At every step, the protein was monitored by reducing 12.5% sodium dodecyl sulfate polyacrylamide gel electrophoresis (SDS-PAGE; Laemmli, 1970) and gels were stained

with silver or coomassie brilliant blue (CBB) R-250 (Figure 2-1-1).

Crystallization

Neuropsin was crystallized by a hanging drop vapor diffusion method at 4℃ (McPherson, 1976). Screening of initial conditions for crystallization was curried out by a sparse matrix approach, Crystal Screen I, II (Hampton Research, USA; Jancarik *et al.*, 1991 and Cudeny *et al.*, 1994). Using polyethylene glycol (PEG) 8000, 4000 or 1500, crystals were obtained in various conditions with a wide range of pH from 5.6 to 8.5 at 4℃. Rod-like crystals (crystal form I) of neuropsin were grown from hanging drops that were made with 0.6 μl of 17 mg/ml protein solution mixed with 0.6 μl of reservoir solution, containing 20% (w/v) PEG 8000 and 50 mM potassium phosphate (Table 2-1-3). Crystals appeared after 4 days and developed to a final size of about 0.1 mm x 0.1 mm x 0.3 mm over a period of two weeks (Figure 2-1-2a). Plate-like crystals (crystal form II) were also grown from 5 μl hanging drops containing 8.3 mg/ml protein with 50 mM HEPES buffer (pH 7.0), 25 mM potassium phosphate, and 10% PEG 8000, against 1 ml of reservoir solution containing 25% PEG 8000 (Table 2-1-3). Needle crystals appeared first and then plate-like crystals began to grow to a final size of about 0.05 mm x 0.1 mm x 0.4 mm over a period of 3 weeks (Figure 2-1-2b).

Data Collection

X-ray diffraction data of crystal form I were collected at 4℃ with an imaging-plate area detector, R-AXIS IV (Rigaku, Japan), using Cu-K_α radiation (λ = 1.54178 Å) generated by a rotating anode generator, FR-C (Rigaku, Japan), operating at 50 kV and 60 mA. The focus size of the X-ray beam was 100 μm and the beam was focused using a double-focusing mirror (Charles Supper, USA). The distance from a crystal to an imaging plate was 100 mm. The data of 180° rotation were collected at a rate of 2° per 30 min for each image. Intensities were evaluated with the program PROCESS (Rigaku,

Japan; Higashi, 1990). Each intensity, *I(h k l)*, was evaluated from the imaging plates and transformed to the amplitude of structure factor, *F(h k l)*, where *h*, *k*, and *l* are the reciprocal lattice points. The crystals belong to the triclinic system, space group *P* 1, with the unit cell dimensions, $a = 97.16$ Å, $b = 97.12$ Å, $c = 46.75$ Å and $\alpha = 99.17°$, $\beta = 99.77°$, $\gamma = 117.35°$ (Table 2-1-4). Intensity data to 3.1 Å resolution was collected with a completeness of 89% and an R_{merge} of 6.7% (Table 2-1-4). The reliability of data, R_{merge}, is defined by,

$$R_{merge} = \frac{\sum_{hkl}\sum_{i}\left|I_i(hkl) - \langle I(hkl)\rangle\right|}{\sum_{hkl}\sum_{i} I_i(hkl)} \times 100,$$

where $I_i(h\ k\ l)$ is the *i*-th measurement and $\langle I(h\ k\ l)\rangle$ is the mean of the measurements. The typical value of R_{merge} is under 10%. An estimation of the number of molecules per unit cell, *Z*, can be made by a V_m value which is the ratio of the unit cell volume and the molecular weight. (Matthews, 1968). The V_m value is given by,

$$V_m = \frac{V_{cell}}{M_r Z},$$

where V_{cell} is the volume of the unit cell and M_r is the molecular weight of the protein. V_m values usually range between 1.7 and 3.5 Å^3/Da. Assuming six neuropsin molecules in the asymmetric unit gives a V_m of 2.5 Å^3/Da. The solvent content of the crystal, V_{solv}, is calculated from V_m values by,

$$V_{solv} = \left(1 - \frac{1.23}{V_m}\right) \times 100,$$

and this scheme gave a V_{solv} of 51%. The self-rotation functions were calculated with the program POLARRFN in the CCP4 package (Collaborative Computational Project Number 4, 1994). Self-rotation function analyses of these data revealed a strong peak (83% of the origin peak) representing a noncrystallographic three-fold axis lying along *c*-axis in the section $\kappa = 120°$ (Figure 2-1-3a), though only weak peaks (32-40% of the origin peaks) were found in the section $\kappa = 180°$ (Figure 2-1-3b). These results indicate

that the asymmetric unit contains two trimeric neuropsin molecules that are related by a three-fold axis, though two-fold symmetry between two trimeric neuropsin molecules is rather poor.

X-ray diffraction data of crystal form II were collected at 4℃ with an imaging-plate area detector, R-AXIS IIc (Rigaku, Japan), using graphite monochromatized Cu-K_α radiation generated by a rotating anode generator, RU-300H (Rigaku, Japan), operating at 40 kV and 100 mA. The focus size of the X-ray beam was 300 μm and the distance from a crystal to an imaging plate was 100 mm. The data of 180° rotation were collected at a rate of 2.5° per 30 min for each image. Intensities were evaluated with the program PROCESS. X-ray diffraction data were also collected at 4℃ at the BL-18B beamline station of the Photon Factory, Tsukuba. The data were recorded using 1 Å radiation, with 200 μm collimated beam, on 200 mm x 400 mm imaging plates (Fuji, Japan) with a Weissenberg camera. The film cassette held one imaging plate that had a crystal-to-film distance of 429.78 mm. Oscillations of ω of 10.0° were used with a speed of 2°/sec. The coupling constant for sliding the cassette, ω/Z, was 2 to 2.5°/mm. A total of 24 Weissenberg photographs were taken, each with an exposure time of 150 sec and an overlap of ω of 0.5°. During data collection, the crystal was slide along the rotation spindle to shift the irradiation point on the crystal. The film images were read by a reader system, BAS 2000 (Fuji, Japan), for production of digitized data. Intensities were evaluated with the program DENZO (Otwinowski, 1993). The crystals belong to the triclinic system, space group $P1$, with the unit cell dimensions a = 38.40 Å, b = 55.16 Å, c = 65.37 Å and α = 95.38°, β = 89.98°, γ = 110.46° (Table 2-1-4). Intensity data to 2.1 Å resolution was collected with a completeness of 93% and an R_{merge} of 6.0% (Table 2-1-4). Assuming two neuropsin molecules in the asymmetric unit give a V_m of 2.5 $Å^3$/Da and a V_{solv} of 53%. Self-rotation function analyses of these data revealed strong peaks (75% of the origin peaks) representing a non-crystallographic two-fold axis lying along a-axis (Figure 2-1-4).

Cross-rotation function analyses between crystal form I and II were also calculated with the program POLARRFN, but gave no significant peak. It is unclear why neuropsin formed a trimer in crystal form I and a dimer in crystal form II. No biochemical evidence was obtained for either the trimeric or dimeric form in solution (Figure 2-1-5).

N-terminal Sequencing and Oligosaccharide Analysis

Five N-terminal sequencing for the crystallized neuropsin was carried out using a protein sequencer system, Model 476A (Applied Biosystems, Inc., USA) and corresponded to the putative sequence for the active-type neuropsin (Figure 2-1-6). Neuropsin has a putative glycosylation site at Asn^{95} of the kallikrein loop. A matrix-assisted laser desorption/ionization time-of-flight (MADLDI-TOF) mass spectrum (PerSeptive Biosystems, Inc., USA) indicated its heterogeneous glycosylation (Figure 2-1-7). Two-dimensional high pressure liquid chromatography (HPLC) mapping revealed that the N-glycans contained 89% paucimannosidic structures with and without attached fucose residue(s) at the innermost *N*-acetylglucosamine (GlcNAc) residues but the glycosylation pattern exhibited high heterogeneity as found on many glycoproteins (Figure 2-1-8).

Phasing with Molecular Replacement Method

The electron density $\rho(x\ y\ z)$ of the crystal is calculated with structure factors, $\mathbf{F}(h\ k\ l)$, by,

$$\rho(xyz) = \frac{1}{V}\sum_h\sum_k\sum_l \mathbf{F}(hkl)e^{-2\pi i(hx+ky+lz)},$$

$$\mathbf{F}(hkl) = F(hkl)e^{i\alpha(hkl)},$$

and,

$$|F(hkl)|^2 = I(hkl),$$

where x, y, and z are relative coordinates in the real space unit cell, and h, k, and l are the reciprocal lattice points. The X-ray diffraction experiments give only the intensities, $I(h\ k\ l)$, yielding to the amplitudes of structure factors, $F(h\ k\ l)$. To obtain the electron density, the phase angles of structure factors, $\alpha(h\ k\ l)$, are needed. There are several techniques to obtain protein crystal phases using heavy atom isomorphous replacement method, anomalous scattering method, or molecular replacement method. The molecular replacement method can be applied if the structure of the protein or homologous proteins was already established. Without phase angles of structure factors, the Patterson function, $P(u\ v\ w)$, can be calculated by Fourier summation with intensities as coefficients,

$$P(uvw) = \frac{1}{V}\sum_{hkl}|F(hkl)|^2 \cos[2\pi(hu + kv + lw)],$$

where u, v, and w are relative coordinates in the Patterson cell, which has dimensions identical to the real cell. The Patterson function can alternatively be written as,

$$P(\mathbf{u}) = \int_{cell} \rho(\mathbf{x})\rho(\mathbf{x}+\mathbf{u})dv.$$

This equation means that the Patterson function will have a large value only if the positions **x** and **x+u** both represent atomic positions, that is when **u** is an interatomic vector. The Patterson function, therefore, represents a map of the interatomic vectors including self-vectors at the origin. If a real unit cell contains N atoms, the corresponding Patterson map will show N(N-1) peaks around the origin. A large number of N such as proteins give too many peaks to interpret, so it is impossible to determine the whole structure from the Patterson function in practice. However, molecules having a similar shape show similar Patterson maps and the known protein molecular structure from its crystalline arrangement can be transferred to the crystal of the protein for which the structure is not yet known by fitting the Patterson functions together. This is the molecular replacement method and involves two steps: *rotation* and *translation*

(Rossmann and Blow, 1962). At first rotation, matrix [C] is needed to determine to maximize an overlap function R(C) defined as,

$$R(C) = \int_U P(\mathbf{u}) P_{\text{model}}([C]\mathbf{u}) d\mathbf{u}.$$

$P(\mathbf{u})$ is the Patterson function of unknown structure, $P_{\text{model}}([\text{C}]\mathbf{u})$ is the model Patterson function, $P_{\text{model}}(\mathbf{u})$, rotated by matrix [C], and U is the volume in the Patterson map where the self-Patterson peaks are located. In the next step, translation vector, **m**, can be determined to maximize another overlap function $T_2(\mathbf{m})$, a translation function (Crowther and Blow, 1967; Crowther, 1972), defined as,

$$T_2(\mathbf{m}) = \int_V P_{\text{model}}(\mathbf{u}) P_{\text{model}}(\mathbf{m},\mathbf{u}) d\mathbf{u}.$$

It results in peaks corresponding to all possible intermolecular vectors in the unknown structure. The model structure contains the same number of molecules as the unknown crystal structure has in its unit cell. $P_{\text{model}}(\mathbf{m}, \mathbf{u})$ is cross-Patterson function between the all molecules existing in the unit cell. $P_{\text{model}}(\mathbf{u})$ is created from the model structure by rotation matrix [C], and **m** is the position vector of one of the molecules existing in the unit cell. The positions of the other molecules are calculated by crystallographic symmetry operations to **m**.

Reliability of the solutions in the molecular replacement method are judged by calculating an R-factor, R, and the correlation coefficient, Cc, defined as,

$$R = \frac{\sum_{hkl} \left| |F_{obs}| - k|F_{calc}| \right|}{\sum_{hkl} |F_{obs}|} \times 100,$$

$$k = \frac{\sum_{hkl} |F_{obs}||F_{calc}|}{\sum_{hkl} |F_{calc}|^2},$$

and,

$$Cc = \frac{\sum_{hkl}\left(|F_{obs}|^2 - \overline{|F_{obs}|^2}\right)\left(|F_{calc}|^2 - \overline{|F_{calc}|^2}\right)}{\sqrt{\sum_{hkl}\left(|F_{obs}|^2 - \overline{|F_{obs}|^2}\right)^2 \sum_{hkl}\left(|F_{calc}|^2 - \overline{|F_{calc}|^2}\right)^2}} \times 100.$$

Both schemes gave the agreement index between calculated structure factors, F_{calc}, and observed structure factors, F_{obs}. The R-factor includes a scale factor k for the intensities, but not for the correlation coefficient, which is scaling insensitive. So the correlation coefficient has an advantage over the R-factor. In the refinement, the R-factor has to be minimized and the correlation coefficient has to be maximized.

The structural analysis was carried out using the intensities data for crystal form II. The initial phases were calculated by the molecular replacement method with the program AMoRe (Navaza, 1994) using a polyalanine model based on the structure of bovine β-trypsin (Chambers and Stroud, 1979; The Protein Data Bank (PDB) code: *4PTP*, The Research Collaboratory for Structural Bioinformatics (RCSB); *http://www.rcsb.org/pdb/*), with which neuropsin shares 38% sequence identity. A summary of the solutions of rotation and translation function with the program AMoRe are given in Table 2-1-5 and 2-1-6.

Model Building and Refinement

Rigid body refinement of the search model were performed with the program X-PLOR (Brünger, 1992). This refinement is the process of refining the positions of rigid groups of atoms against the observed amplitudes and is often done as a first step in a refinement procedure after the molecular replacement procedure has given starting values for the position and orientation of the model. The protein model was divided into two or four groups and each group was refined with the six parameters, three rotations and three translations, according to the R-factors and the correlation coefficients described above. Followed by rigid body refinements, solvent flattening/histogram matching with the program DM (Cowtan and Main, 1996) were also performed. Solvent flattening is

based on the assumption that a structure factor from crystal is a summation of those from protein and solvent region,

$$\mathbf{F}_{crystal} = \mathbf{F}_{protein} + \mathbf{F}_{solvent},$$

and one can get improved $\mathbf{F}_{crystal}$ by refining not only $\mathbf{F}_{protein}$ but also $\mathbf{F}_{solvent}$. In the highly refined protein crystal structures, it is known that the electron density map of the solvent region is rather flat compared to protein region. Except around the protein, the solvent has dynamic nature and its time-averaged electron density has a low constant value. If the protein region can be identified, the rest density should be set to a low constant value. After solvent flattening, amplitudes and phases for a new structure factor are calculated using the Fourier transform of density and the new electron density map is calculated with these improved phase angles. In this study, the molecular envelope around the protein was defined by visual inspection from the preliminary electron density map using the model phases. Histogram matching is another method which modifies the electron density map, and based on the empirical fact that electron density maps of well-refined proteins have similar histograms to each other when they have the same resolution range and similar solvent contents. To make the histogram, the grid points of the electron density map are grouped by their density sizes into the same interval ranges and the number in the same range is counted. The obtained histogram is fitted onto the ideal histogram which is calculated under the same resolution range and solvent content. This modified electron density is put back to the grid points, and new structure factors are calculated. Six regions of insertions and deletions were inspected on the resulting $2F_o$-F_c map, which was generated with the program O (Jones *et al.*, 1991). $2F_o$-F_c map is the calculated electron density using $2|F_{obs}|$ - $|F_{calc}|$ as Fourier coefficients, written as,

$$\rho(xyz) = \frac{1}{V}\sum_{hkl}\left(2|F_{obs}| - |F_{calc}|\right)e^{[-2\pi i(hx+ky+lz)+i\alpha_{calc}]},$$

where α_{calc} are the phase angles calculated for the model. This map can be regarded as the sum of the electron density of the model and of excessive electron densities at normal

height and provides informations for the unknown structures which are not included or are wrong in the model. Residues in these regions were also inspected on their omit maps. Omit map is $2F_o$-F_c map calculated with a model which is excluded doubtful regions and introduced slight random shifts to reduce model bias.

The structure was built and refined through simulated annealing cycles with the program O and X-PLOR, respectively. Simulated annealing method is using molecular dynamics technique, in which the dynamic behavior of a system of particles is simulated. This simulation yields to an ensemble of structures that is energetically allowed for given temperature and pressure. The energy of the structures distribute followed by Bolzmann's law, which states that the number of structures with a potential energy ε_{pot} is proportional to $\exp[-\varepsilon_{pot}/k_0T]$, where k_0 is Boltzmann's constant and T is the absolute temperature. The potential energy depends on the relative positions of the atoms and is calculated on the basis of known potential energy functions. A molecular dynamics calculation on a molecule starts with assigning to the atoms velocities derived from a Maxwelloan distribution at an appropriate temperature. At time $t = 0$, the atoms are in a starting configuration that has a potential energy E_{pot} for the entire molecule. On each atom i at position r_i, and mass m_i, two forces which are calculated based on the derivative of the potential energy and Newtonian mechanics will be equal,

$$-E_{pot}/r_i = m_i\left(d^2r/dt^2\right).$$

After a short time step Δt, usually in the 10^{-15} sec range, the process is repeated with the atoms in the new positions, and this cycle is repeated until E_{pot} reaches to the minimum, usually after 10^3-10^4 times. Actual function to be minimized is the total energy of the system, Q, which includes a crystallographic discrepancy term E_{Xray} as a pseudoenergy and a potential energy E_{pot} for the entire molecule calculated both as above and below,

$$Q = E_{Xray} + E_{pot},$$

where,

$$E_{Xray} = w_{Xray} \sum_{hkl} \left(|F_{obs}| - k|F_{calc}| \right)^2,$$

and,

$$E_{pot} = E_{bond} + E_{bond\ angle} + E_{torsion} + E_{dihedral} + E_{van\ der\ Waals} + E_{electrostatic}.$$

w_{Xray} is a weighting factor which controls the relative contribution of the potential energy and X-ray pseudoenergy, and is chose according to balance between the final r.m.s. deviations due to E_{pot} alone and those due to E_{Xray} alone after performing short molecular dynamics simulations with one energy alone. E_{pot} includes the potential energies of bond stretching, E_{bond}, bond angle bending, $E_{bond\ angle}$, torsion potentials, $E_{torsion}$, van der Waals interactions, $E_{van\ der\ Waals}$, and electrostatic potentials, $E_{electrostatic}$.

Two regions were poorly defined in the resulting map. One is at the loop residues, Arg^{74} and Asp^{75}, and the other is at the three C-terminal residues. These residues have uninterpretable densities implying complex disorder. The current structure contains 450 amino acid residues, 2 sugars, and 194 waters. The R-factor is 18.6% (a free R-factor of 22.7%; Brünger, 1996) for all reflections to 2.1 Å resolution. There is no residue in disallowed region as defined in the program PROCHECK (Laskowski, 1993), but 89.4% residues in the most favorable regions and 10.6% residues in the additional allowed regions (Figure 2-1-10). The final refinement statistic are shown in Table 2-1-7.

Table 2-1-1 TNM-FH Medium with 10% Fetal Calf Serum

Grace's Insect Cell Medium Powder	46.3 g
Yeastlate	3.3 g
Lactoalbumin Hydrate	3.3 g
Gentamycin Sulfate	50 mg
D.W.	
Adjust pH 6.2 and measure up to 1 liter.	
Add to	
Heat-inactivated Fetal Calf Serum	100 ml

This medium was sterilized using a filter (0.22 μm) and stored at 4℃.
This medium was heated at 27℃ just before use.

Table 2-1-2 Serum-free Medium

Sf-900II SFM Powder	38.1 g
Sf-900II Supplement	0.8 ml
$NaHCO_3$	0.35 g
Gentamycin Sulfate	50 mg
D.W.	

Adjust pH 6.2 and measure up to 1 liter.

This medium was sterilized using a filter (0.22 μm) and stored at 4℃.
This medium was heated at 27℃ just before use.

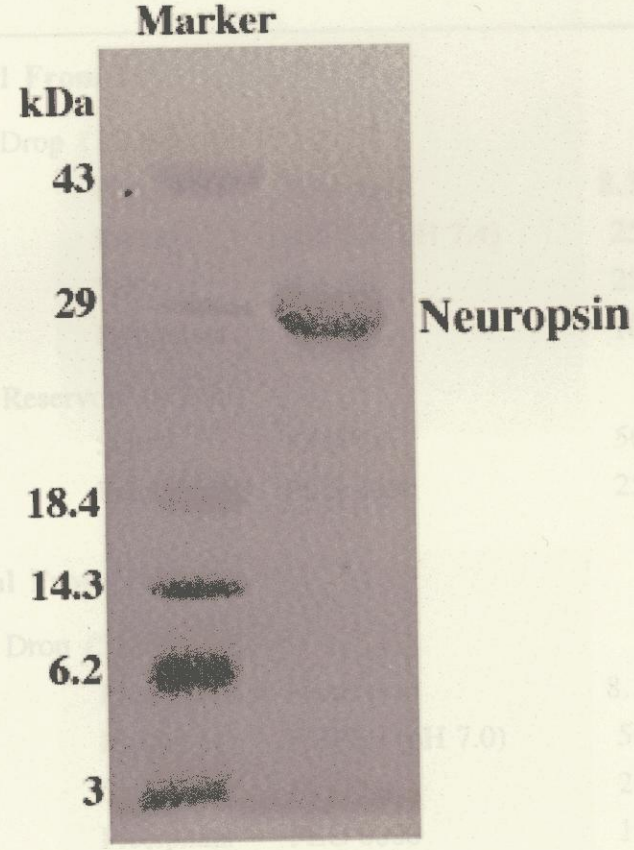

Figure 2-1-1 Purification of Neuropsin Purified neuropsin was subjected to reducing 12.5% SDS-PAGE and stained with CBB R-250.

Table 2-1-3 Crystallization Conditions of Neuropsin Crystals

Crystal From I		
Drop (1.2 μl)		
Protein	Neuropsin	8.3 mg/ml
Buffer	HEPES (pH 7.4)	25 mM
Salt	KH_2PO_4	25 mM
Precipitant	PEG 8000	10 % (w/v)
Reservoir (0.5 ml)		
Salt	KH_2PO_4	50 mM
Precipitant	PEG 8000	25 % (w/v)
Crystal From II		
Drop (5 μl)		
Protein	Neuropsin	8.3 mg/ml
Buffer	HEPES (pH 7.0)	50 mM
Salt	KH_2PO_4	25 mM
Precipitant	PEG 8000	10 % (w/v)
Reservoir (1 ml)		
Precipitant	PEG 8000	25 % (w/v)

Temperature is 4℃.

a

b

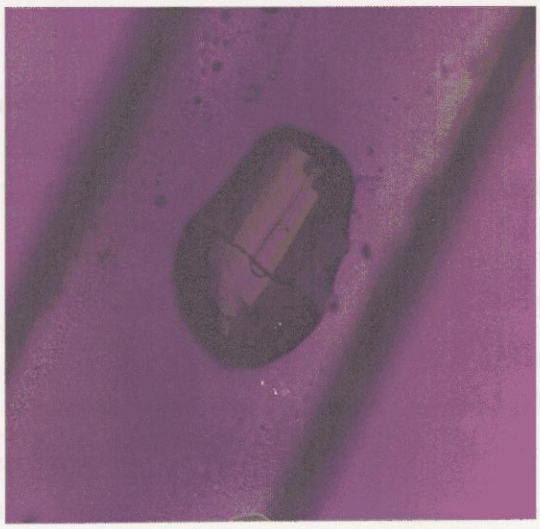

Figure 2-1-2 Crystals of Neuropsin *a*, Rod-like crystals (crystal form I) of neuropsin *b*, A plate-like crystal (crystal form II) of neuropsin

Table 2-1-4 Crystal Data and Data Collection Statistics of Neuropsin Crystals

Crystal Form I		
Crystal Data		
Crystal System	Triclinic	
Space Group	*P* 1	
Unit Cell Dimensions	*a* = 97.16 Å	α = 99.17°
	b = 97.12 Å	β = 99.77°
	c = 46.75 Å	γ = 117.35°
Z	6	
V_m	2.5 Å³/Da	
V_{solv}	51%	
Data Collection Statistics		
Resolution	3.1 Å	
R_{merge}	6.7% (13.4%)[1)]	
Number of Measured Reflections	37,416	
Number of Independent Reflections	25,348	
Completeness	89% (76%)[1)]	
Mean<I/σ(I)>	12.0 (5.0)[1)]	
Crystal Form II		
Crystal Data		
Crystal System	Triclinic	
Space Group	*P* 1	
Unit Cell Dimensions	*a* = 38.40 Å	α = 95.38°
	b = 55.16 Å	β = 89.98°
	c = 65.37 Å	γ = 110.46°
Z	2	
V_m	2.6 Å³/Da	
V_{solv}	53%	
Data Collection Statistics		
Resolution	2.1 Å	
R_{merge}	6.0% (19.8%)[2)]	
Number of Measured Reflections	69,767	
Number of Independent Reflections	24,944	
Completeness	90% (67%)[2)]	
Mean<I/σ(I)>	8.5 (3.1)[2)]	

[1)] Outer shell is from 3.1 to 3.2 Å. [2)] Outer shell is from 2.1 to 2.2 Å.

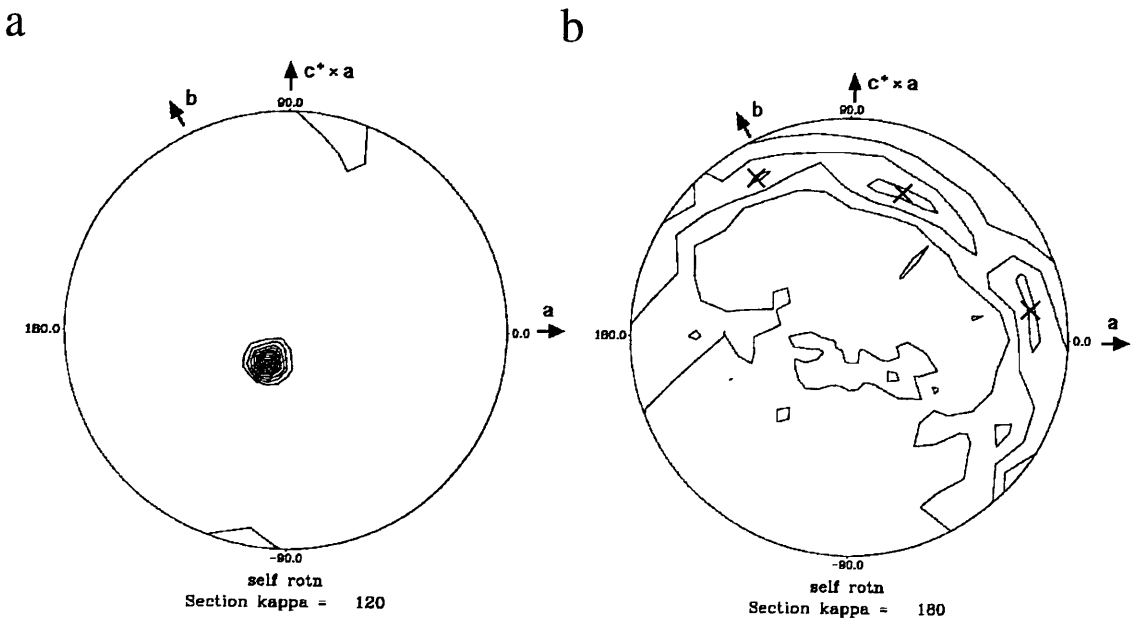

Figure 2-1-3 Stereographic Projection of the Self-rotation Function for Neuropsin Crystal Form I Integration radius in Patterson space is 17 Å and data are included from 15 to 3.0 Å. Contouring starts at the 2σ level and the interval is 1σ. *a*, The section κ = 120° of the self-rotation function. A peak at ω = 19.4°, ϕ = -122.7° corresponds to the noncrystallographic three-fold axis along the *c*-axis. *b*, The section κ = 180° of the self-rotation function. Three peaks at ω = 76.1°, ϕ = 18.7°; ω = 71.8, ϕ = 80.1°; and ω = 88.6°, ϕ = 140.1° correspond to the noncrystallographic two-fold axes perpendicular to the *c*-axis. These peaks are marked by crosses.

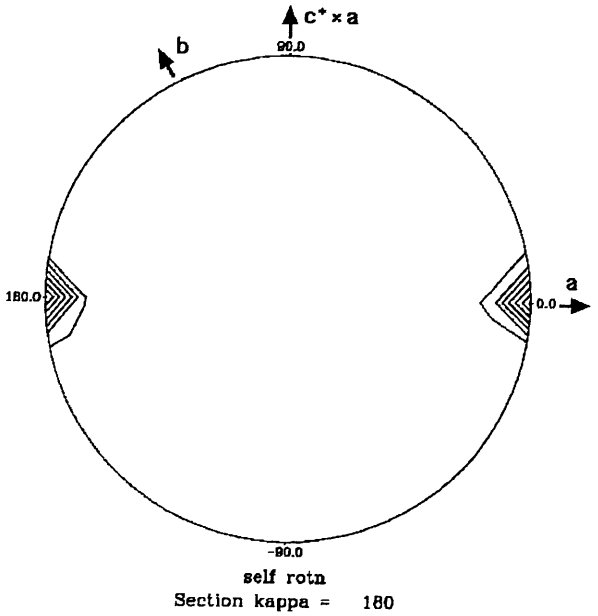

Figure 2-1-4 Stereographic Projection of the Sections κ = 180° the Self-rotation Function for Neuropsin Crystal Form II Two peaks at ω = 90°, ϕ = 0° and ω = 90°, ϕ = 180° correspond to the noncrystallographic two-fold axis perpendicular to the *a*-axis. Integration radius and contouring level are the same as in Figure 2-1-3.

a

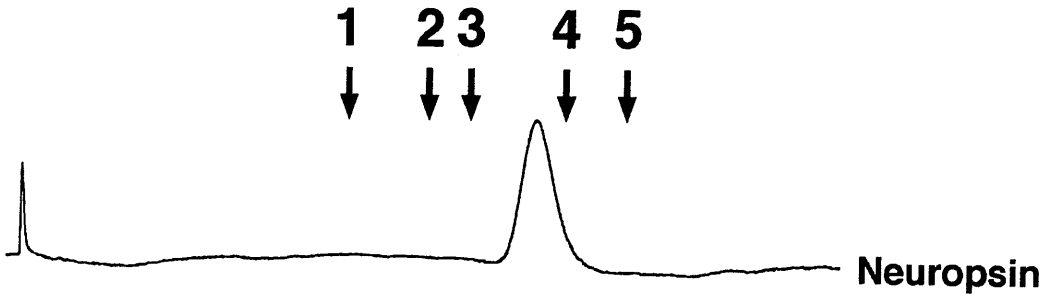

b

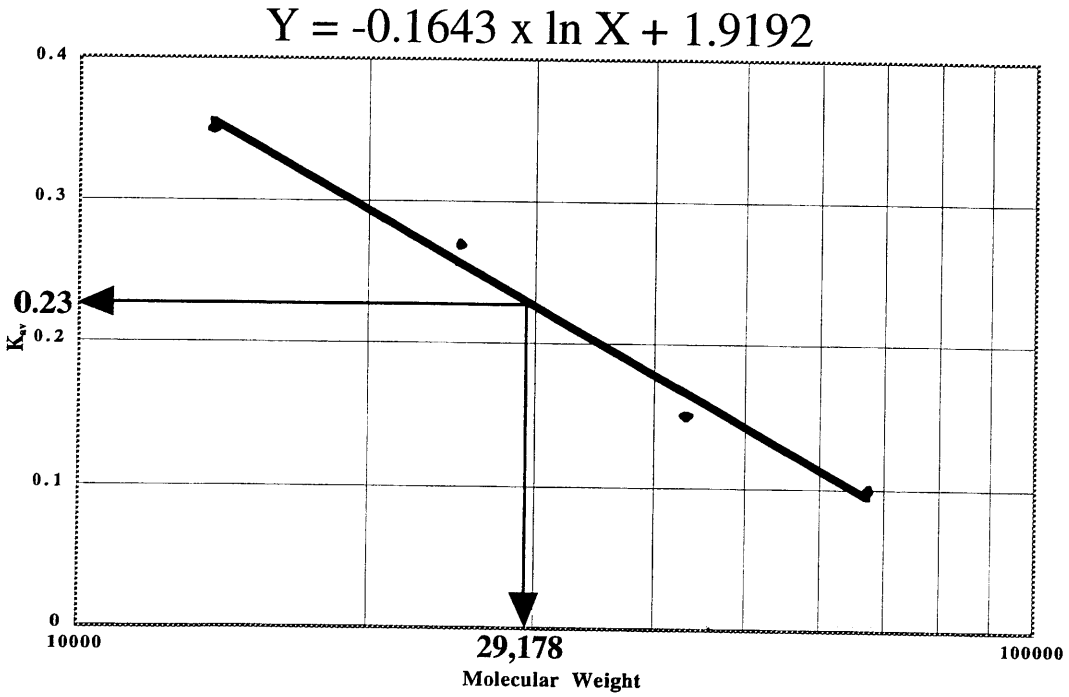

Figure 2-1-5 Molecular Weight Determination of Neuropsin in Solution
a, An elution pattern of neuropsin by gel filtration. The molecular weight of neuropsin in solution (10 mM HEPES pH 7.4, 150 mM NaCl) was determined using a gel filtration column, Superdex 75 HR 10/30 (V_t: 24 ml; Amersham Pharmacia Biotech, UK) and five molecular weight markers, which include blue dextran 2000 (M_r:> $2x10^6$ for checking void volume, V_e: 7.10 ml; arrow No.1), albumin (M_r: 67,000, V_e: 8.80 ml; arrow No.2), ovalbumin (M_r: 43,000, V_e: 9.65 ml; arrow No.3), chymotrypsinogen A (M_r: 25,000, V_e: 11.63 ml; arrow No.4), and ribonuclease A (M_r: 13,700, V_e: 12.95 ml; arrow No.5). Flow rate of the buffer is 0.5 ml/min and chart speed is 1 cm/ml. *b*, Plots of molecular markers. The molecular weight of neuropsin was estimated by plotting the K_{av} (= V_e-V_0/V_t-V_0) on a calibration curve (K_{av} vs. molecular weight) with the markers. The obtained molecular weight for neuropsin (V_e: 11.02 ml, K_{av}: 0.23) in solution was estimated about 29,178, which shows that neuropsin is a monomer in solution.
(continued)

V_0: void/exclusion volume
V_t: total bet volume
V_e: elution volume of sample
K_{av}: coefficient describing the fraction of stationary gel volume available for diffusion of a given species

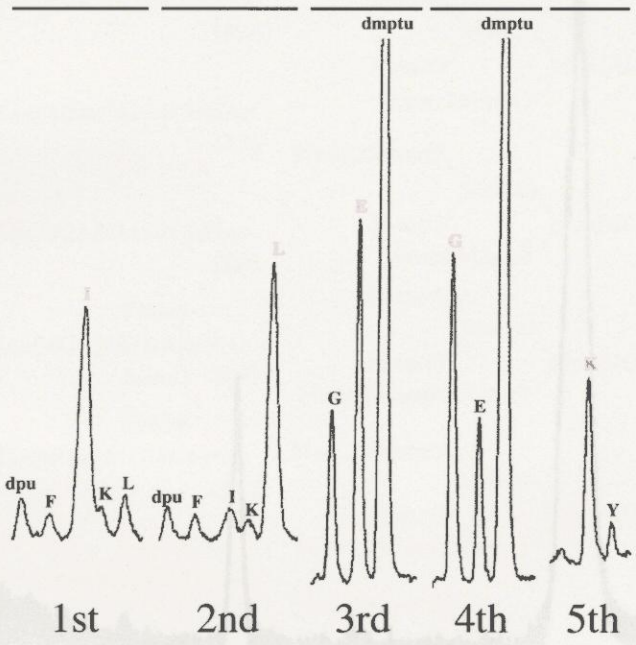

Figure 2-1-6 An N-terminal Sequence of Crystallized Neuropsin
Neuropsin was degraded using the Edman's method and eluted with an HPLC. Each amino acid peak is shown using one letter symbol. Red letters show the estimated sequence, which is identical to the N-terminal sequence of the active-type neuropsin (Ile^{16}-Leu^{17}-Glu^{18}-Gly^{19}-Lys^{20}).

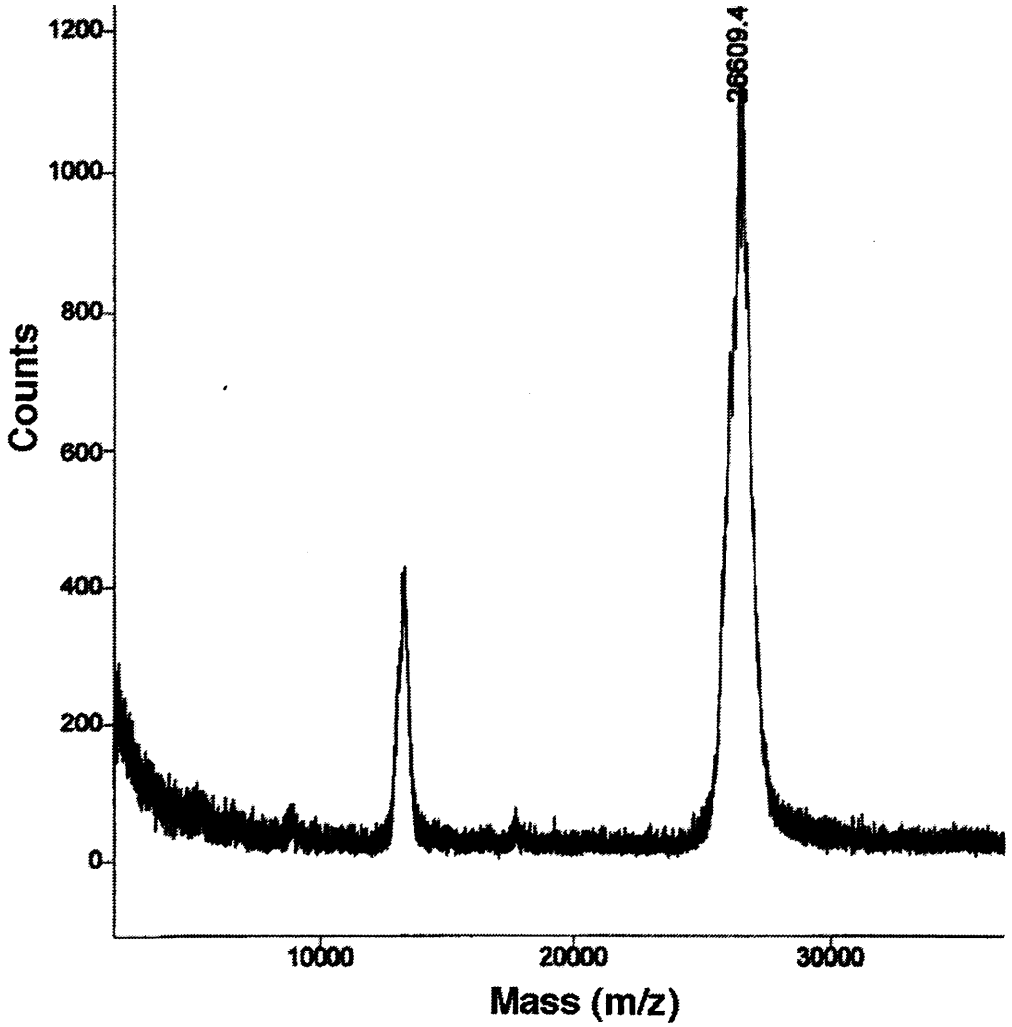

Figure 2-1-7 An MADLDI-TOF Mass Spectrum of Neuropsin Neuropsin had heterogeneous mass spectrum to be estimated about M_r: 26,609.4 because of heterogeneous glycosylation.

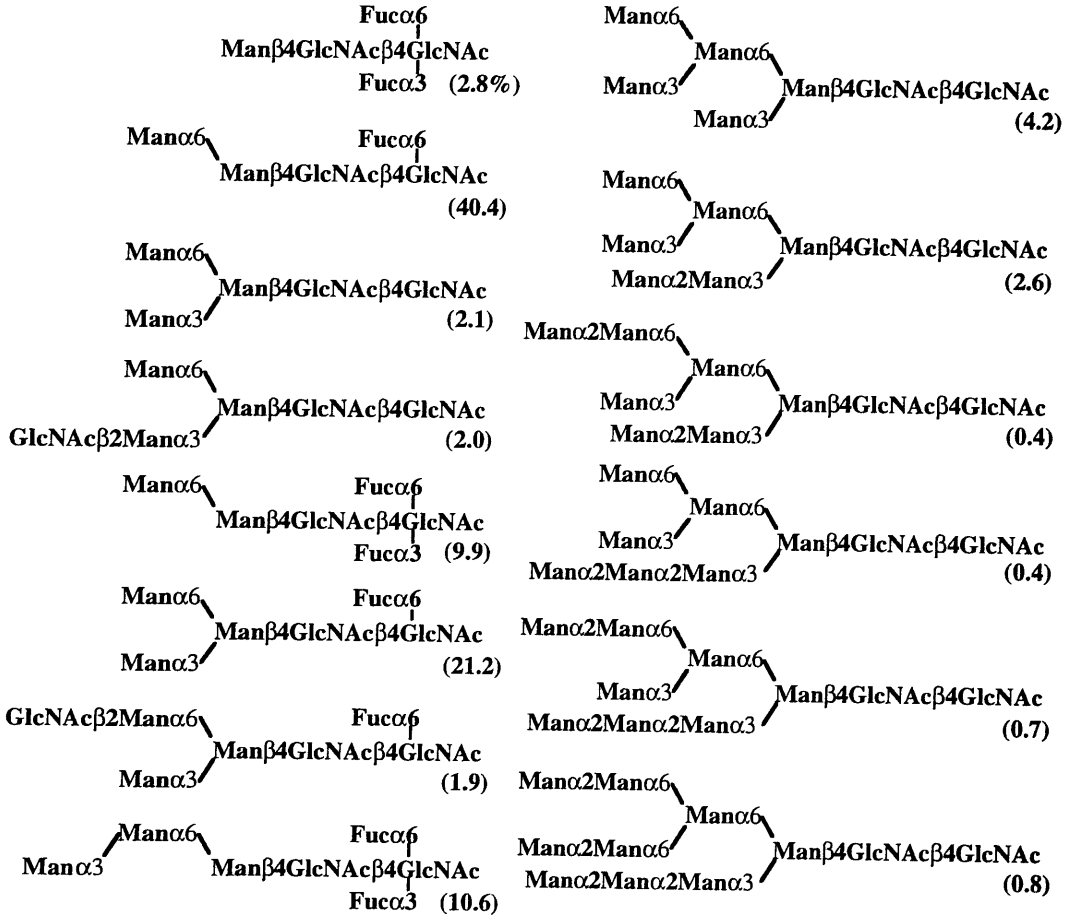

Figure 2-1-8 Estimated Structures of Oligosaccharides Obtained from Neuropsin Expressed in High Five Insect Cells. Fourteen types of oligosaccharides were separated by an HPLC using standard two-dimensional sugar mapping technique. Each numerical value in parenthesis shows the relative quantity.

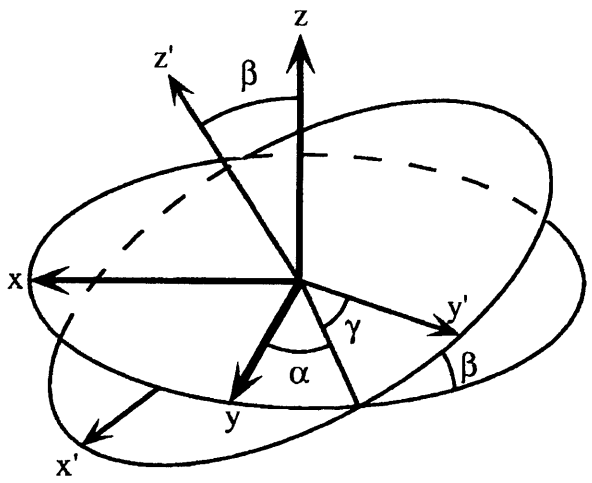

Figure 2-1-9 The Definition of the Eulerian Angles A direction of a molecule is shown using three angles, the Eulerian angles (α, β, and γ).

Table 2-1-5 The Solutions of Rotation Function for Crystal Form II

	α	β	γ	*Cc*
1	213.97	74.98	46.29	26.80
2	145.91	104.98	226.22	26.80
3	6.81	109.46	323.72	18.80
4	353.47	70.28	143.50	18.40
5	163.65	108.86	270.35	18.20
6	196.39	70.94	90.24	18.00
7	339.46	141.34	152.81	17.70
8	20.81	39.32	333.50	17.20
9	196.76	27.31	86.44	17.20
10	163.07	152.44	266.48	17.10

The best ten solutions are shown. These solutions were calculated with the program AMoRe with integration radius = 25 Å and data included from 15 to 6.0 Å. Correlation coefficients (*Cc*) of the 1st and 2nd solutions are remarkably large. α, β, and γ are shown the Eulerian angles (see Figure 2-1-9).

Table 2-1-6 The Solutions of Translation Function for Crystal Form II

	α	β	γ	x	y	z	*Cc*	*R*
1	145.91	104.98	226.22	0.6482	0.2987	0.5734	52.0	43.3
2	145.91	104.98	226.22	0.0745	0.1525	0.5559	38.1	47.3
3	145.91	104.98	226.22	0.7188	0.4700	0.1084	36.3	49.2
4	145.91	104.98	226.22	0.8745	0.2490	0.0753	36.2	49.2
5	213.97	74.98	46.29	0.5761	0.5300	0.1872	36.2	48.1
6	145.91	104.98	226.22	0.3713	0.2448	0.0764	36.1	49.5
7	145.91	104.98	226.22	0.1923	0.3911	0.5890	35.9	48.4
8	145.91	104.98	226.22	0.3412	0.6713	0.3250	35.7	49.4
9	145.91	104.98	226.22	0.4312	0.8630	0.1825	35.6	49.8
10	145.91	104.98	226.22	0.6863	0.8957	0.3416	35.6	48.3

The relative position of 2nd neuropsin was calculated on condition that the 1st solution for rotation function (see Table 2-1-5) is fixed. α, β, and γ are shown the Eulerian angles (see Figure 2-1-9). x, y, and z are shown the relative position assuming that each side length in the unit cell is 1. Correlation coefficient (*Cc*) of the best solution is remarkably large and R-factor (*R*) of that is remarkably small.

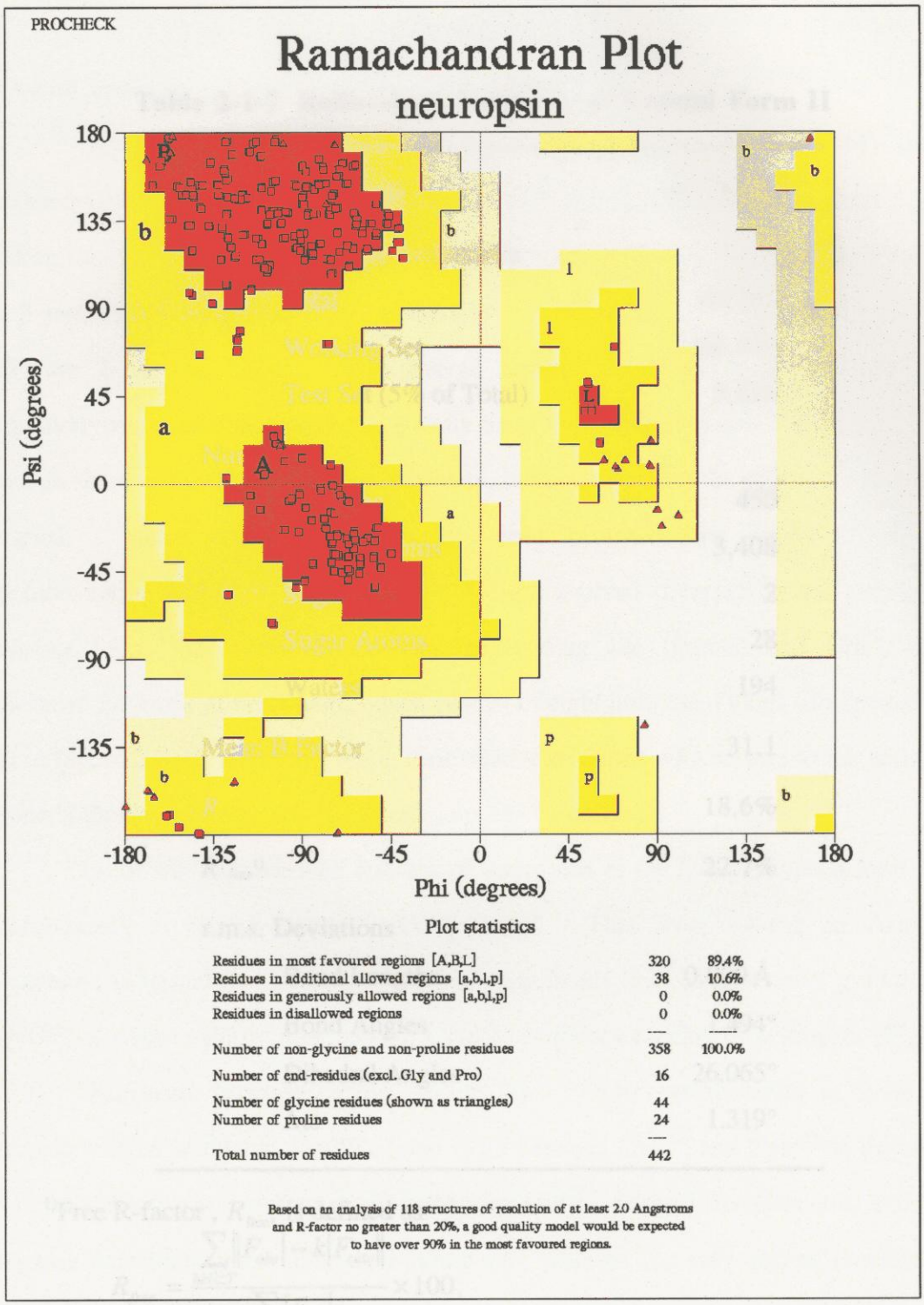

Figure 2-1-10 The Ramachandran Plot of a Neuropsin Model The torsion angles about the C_α-N bond (ϕ) and the C_α-C bond (ψ) of each of its amino acid residue are plotted. This plot shows that this model is appropriate because 89.4% of the residues without glycine and proline are in the most favoured regions (orange areas) at 2.1 Å.

Table 2-1-7 Refinement Statistics of Crystal Form II

Resolution Range	∞ - 2.1 Å
Number of Used Reflections	
Total	69,767
Working Set	66,279
Test Set (5% of Total)	3,488
Number of	
Residues	450
Protein Atoms	3,408
Sugars	2
Sugar Atoms	28
Waters	194
Mean B Factor	31.1
R	18.6%
R_{free} [1)]	22.7%
r.m.s. Deviations	
Bond Lengths	0.009 Å
Bond Angles	1.494°
Dihedral Angles	26.065°
Δω	1.319°

[1)]Free R-factor , R_{free}, is defined as

$$R_{free} = \frac{\sum_{hkl \subset T} \left\| |F_{obs}| - k|F_{calc}| \right\|}{\sum_{hkl \subset T} |F_{obs}|} \times 100,$$

where $h\ k\ l \subset T$ means all reflections belonging to test set T of unique reflections (Brünger, 1996).

2-2. RESULTS

Overall Structure

Neuropsin consists of fourteen β-strands (designated as β1-β14) that are extensively twisted, two α-helices (designated as α1 and α2), and one short 3_{10}-helix (designated as 3_{10}). Each seven β-strands forms an antiparallel β-barrel domain folded in a β-sandwich with a cleft where the catalytic triad (Asp^{57}, His^{102}, and Ser^{195}) is located (Figure 2-2-1 and 2-2-2). This overall structure is homologous to those of the chymotrypsin-type serine proteases (family S1 of the endopeptidases; Barrett *et al.*, 1998), which share an identical catalytic mechanism, but among which the substrate specificity is varied. Many known structures of these proteases are strongly conserved, demonstrating that their variety is caused from evolved diversity in the structures of surface loops that surround the substrate-binding site (Perona and Craik, 1997). Because the loops of neuropsin, which consist of eight prominent loops (designated as A-H in Figure 2-2-1), are conserved in their relative positions with respect to the active site, general themes for their individual functions can be derived.

One of the characteristic features of neuropsin is the *N*-glycosylated loop D that corresponds to the so-called "kallikrein loop". This loop, having an Asn-X-Ser sequence, is typical for members of the kallikrein family that contains nerve growth factor (NGF)-γ, which exhibits relatively high (46%) sequence identity to neuropsin (Figure 2-2-3). Neuropsin, however, forms six disulfide bonds corresponding to those of β-trypsin with an additional disulfide bond (SS3 between Cys^{128} and Cys^{232} in Figure 2-2-1) that is missing in members of the kallikrein family. Large differences exist in the loop regions surrounding the substrate-binding site, whereas the core region contains only minor variations. Excluding the insertional and deletional residues, the main-chain atoms of neuropsin superimpose on the corresponding atoms of bovine pancreatic β-trypsin (PDB code: *4PTP*; Chambers and Stroud, 1979), mouse submaxillary gland NGF-γ in 7S NGF (PDB code: *1SGF*; Bax *et al.*, 1997), an $\alpha_2\beta_2\gamma_2$ complex of NGF, and porcine

pancreatic kallikrein A(PDB code: *2PKA*; Bode *et al.*, 1983) with r.m.s. deviations of 1.26, 1.43, and 1.84 Å, respectively (Table 2-2-1). The geometry of the catalytic triad is highly similar to those of the serine proteases with r.m.s. deviations in a range of 0.2-0.24 Å (Figure 2-2-4). The atomic coordinates and structure factors for neuropsin have been deposited in the RCSB (PDB code: *1NPM*).

S1 Site

Enzyme assay using several 4-methylcoumaryl-7-amide (MCA) or *p*-nitroanilide (*p*NA) derivatives of oligopeptides (Shimizu *et al.*, 1998) has shown that neuropsin has a strong tendency to cleave peptide bonds at C-terminal to arginine or lysine. This primary specificity is well interpreted by the structure of the S1 pocket, a deep cylindrical pocket that is formed by the two loops, G and H, and punctuated at its base by the side chain of Asp^{189}. However, neuropsin has large conformational changes of the loop G with maximum displacements of 4.8-5.8 Å compared with those of NGF-γ, kallikrein, and β-trypsin (Figure 2-2-5 and 2-2-6). The conformational changes in neuropsin seem to be caused by the one-residue (Gly^{186B}) deletion in the loop G. In addition, the loop H of neuropsin also displays large displacements from these proteases because the loop H is heavily interacted with the loop G in all the proteases (Chambers and Stroud, 1979; Bode *et al.*, 1983; Bax *et al.*, 1997). It is noteworthy that the loop H of β-trypsin has a one-residue deletion of the *cis*-proline, Pro^{219}, that is conserved in neuropsin and the kallikrein family containing NGF-γ (Bode *et al.*, 1983; Bax *et al.*, 1997). This deletion induces a larger displacement of neuropsin the loop H from β-trypsin (4.3 Å) than from NGF-γ (3.4 Å) or kallikrein (3.2 Å). Interestingly, the P1 specificity of neuropsin for arginine is comparable with that for lysine. This is in sharp contrast to NGF-γ, kallikrein, and β-trypsin, in which a significant preference for arginine exists. Among key residues of the S1 pocket, Gly^{226} of neuropsin has relatively large displacements from NGF-γ (0.7 Å) and kallikrein (1.2 Å). Alternatively, Ser^{217} of neuropsin has a relatively large

displacement from β-trypsin (1.3 Å). Compared with NGF-γ, the changes of the neuropsin loop structures result in positional displacements (0.4-0.8 Å) of Asp^{189}, Thr^{190}, and His^{217}, which have been reported to form hydrogen bonds to the P1 arginine (Arg^{118}) of NGF-β in 7S NGF-γ (Bax *et al.*, 1997). These local differences may be responsible for the unique P1 specificity of neuropsin. Like other serine proteases, which are activated by cleavage of the peptide bond between Arg^{15} and Ile^{16}, neuropsin tucks the newly formed amino group of Ile^{16} into the pocket to form multiple hydrogen bonds with the main chains of the loop E and to form an ion pair with Asp^{194} of the loop G.

Kallikrein Loop

The kallikrein loop of neuropsin differs radically from those of NGF-γ and kallikrein. In these members of the kallikrein family, the loop was cleaved into the highly mobile nicked chains (Bode *et al.*, 1983; Bax *et al.*, 1997). In contrast, the loop of neuropsin is packed into an ordered and relatively compact conformation without any nicked site: neuropsin has no arginine or lysine residue in the loop. Recently determined crystal structure of mouse glandular kallikrein-13 (PDB code: *1AO5*; Timm, 1997) shows an ordered kallikrein loop, but no conformational similarity with the loop of neuropsin. It seems unlikely that the N-glycan bound to Asn^{95} participates directly in the substrate binding because the GlcNAc residue and the residual density are oriented away from the active site as in members of the kallikrein family (Figure 2-2-7 and 2-2-8).

S2 Site

The kallikrein loop of neuropsin overhangs toward the active site cleft with a prominent Pro^{95D} residue, which suggests its role in substrate binding. Interestingly, superposition of neuropsin on porcine pancreatic β-trypsin complex with soybean trypsin inhibitor (STI) (PDB code: *1AVW*; Song and Suh, 1998) revealed steric clashes between the kallikrein loop of neuropsin and the two STI loops facing toward neuropsin (Figure 2-

2-9). This was borne out by biochemical experiments in which high molecular weight inhibitors, such as STI or α-antitrypsin, were found to have little effect on the neuropsin activity, whereas low molecular weight inhibitors, such as leupeptin, markedly inhibited the activity (Shimizu *et al.*, 1998). The overhanging kallikrein loop forms a narrow pocket (the S2 site) in which Asp^{102} is positioned at the base and would restrict the size of the side chain in the P2 position of substrate peptides. This is consistent with the results of a previous enzyme assay (Shimizu *et al.*, 1998), in which high activities of neuropsin were observed for peptide substrates having smaller residues or proline in the P2 positions. It has been well demonstrated by the crystal structure of thrombin complex with D-Phe-Pro-Arg-chloromethylketone that the loop B of thrombin compresses the S2 site with the inserted residues, Tyr^{60A} and Trp^{60D}, to deduce the P2 specificity of the enzyme for proline (PDB code: *1ABJ*; Bode *et al.*, 1989). Superposition of neuropsin on thrombin shows Pro^{95D} of neuropsin located nearby Tyr^{60A} and Trp^{60D} of thrombin, but no contact between Pro^{95D} and the proline residue of D-Phe-Pro-Arg bound to thrombin, which suggests that the P2 preference for proline may be mediated by the kallikrein loop of neuropsin, instead of the loop B of thrombin, but rather weaker than that of thrombin (Figure 2-2-10). Phenylalanine at the P2 position remarkably reduces the neuropsin activity (Shimizu *et al.*, 1998), which is one of the major differences from kallikrein and NGF-γ.

S3/4 Site

Most striking is the structure of the loop F that is similar to that of β-trypsin rather than NGF-γ and kallikrein, where significant conformational changes of the loop F from neuropsin occur with large displacements, 5.2 and 6 Å, respectively, accompanied by movements of helix α1 (Figure 2-2-5 and 2-2-6). The Loop F is one of the main elements forming the S3/S4 site. It is notable that this loop has Tyr^{172}, which forms hydrogen bonds with the main chains of the loop H and which is conserved in β-trypsin

but is replaced by histidine in NGF-γ and kallikrein. This residue has been elucidated to be one of the distal determinant residues for the substrate specificity (Hedstrom *et al.*, 1994). Moreover, Gly^{174}, which is conserved in neuropsin and β-trypsin, is one of the key residues for the loop F structure because this residue is an essential component of the type-II reverse turn, Tyr-Pro-Gly-Lys. It should be pointed out that the disulfide bond SS3, which is conserved in β-trypsin as already mentioned, may contribute to the conformational resemblance of the loop F with that of β-trypsin through contacts with the strand β13 that associated with the C-terminal β-strand of the loop F, β11.

It is remarkable that the above differences in the loop F may also be correlated with the conformational differences in the kallikrein loops. In NGF-γ and kallikrein, the highly mobile kallikrein loops heavily interact with the loop F although the kallikrein loop of neuropsin has no direct interaction with the loop F, as it does with the loop D of β-trypsin. One of the interesting consequences of these conformational characteristics in the loop D and F is that the S3/S4 site of neuropsin is similar to that of β-trypsin rather than NGF-γ. The aromatic rings of Trp^{215}, Tyr^{172}, and His^{99} provide a shallow but wide hydrophobic depression for the S3/S4 site as in β-trypsin and could explain the high activities of neuropsin observed for synthetic tripeptide substrates having hydrophobic residues in the P3 position. Moreover, in neuropsin, Lys^{175} of the loop F is projected toward the S3/S4 site (Fig 2-2-5, whereas Lys^{175} of NGF-γ is projected away from the S3/S4 site. It is interesting that Lys^{175} may play a role in the P3/P4 interaction with the substrates. Actually, one of the cleavage sites of fibronectin (Shimizu *et al.*, 1998), which is an extracellular matrix protein exhibiting strong proteolytic sensitivity for neuropsin, had the N-terminal sequence of Asp-Val-Arg, whose acidic residue at the P3 position may interact with Lys^{175}.

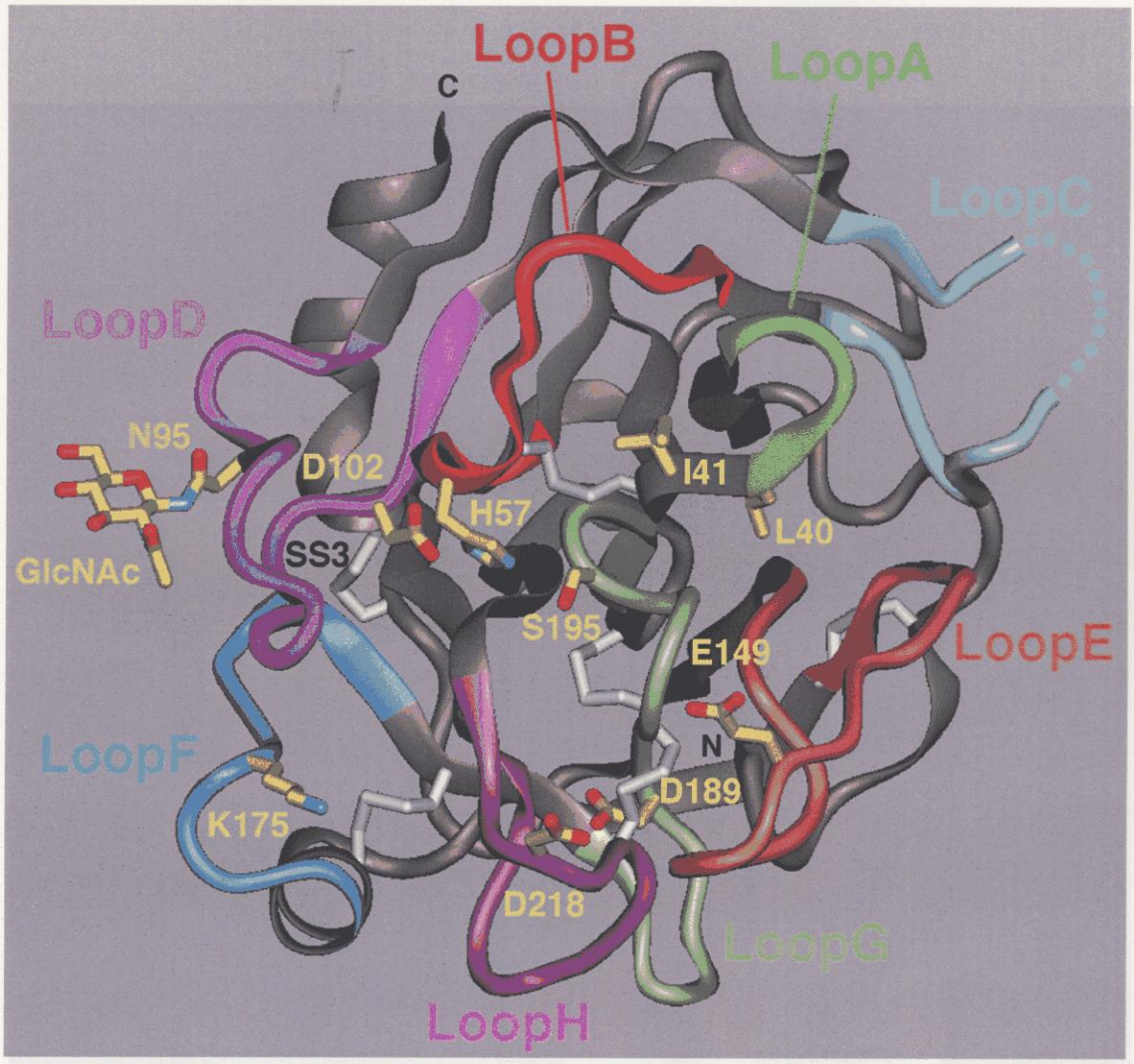

Figure 2-2-1 Overall Structure of Neuropsin (Ribbon Diagram) Seven-straned β-sheets (the top and bottom halves) sandwiches with the catalytic triad at the cleft of the β-sandwich. The surface loops (A-H) forming the substrate-binding site are colored with labels. Six disulfide bonds are shown by bridges in white, and the disulfide bond (SS3), which is conserved in β-trypsin but not in kallikrein, was labeled. The loop D is the kallikrein loop that has *N*-glycosylated Asn^{95} with one visible GlcNAc residue. The side chains of the catalytic triad (His^{57}, Asp^{102}, and Ser^{195}), Asp^{189} at the S1-specific pocket, Lys^{175} at the S3/4 site, Glu^{149} and Asp^{218} at the rim of the S1 pocket, and Leu^{40}, and Ile^{41} at the S1' site, are also shown with stick representations with one-letter amino acid labels. This diagram was drawn with the program QUANTA (Molecular Simulations, Inc., USA).

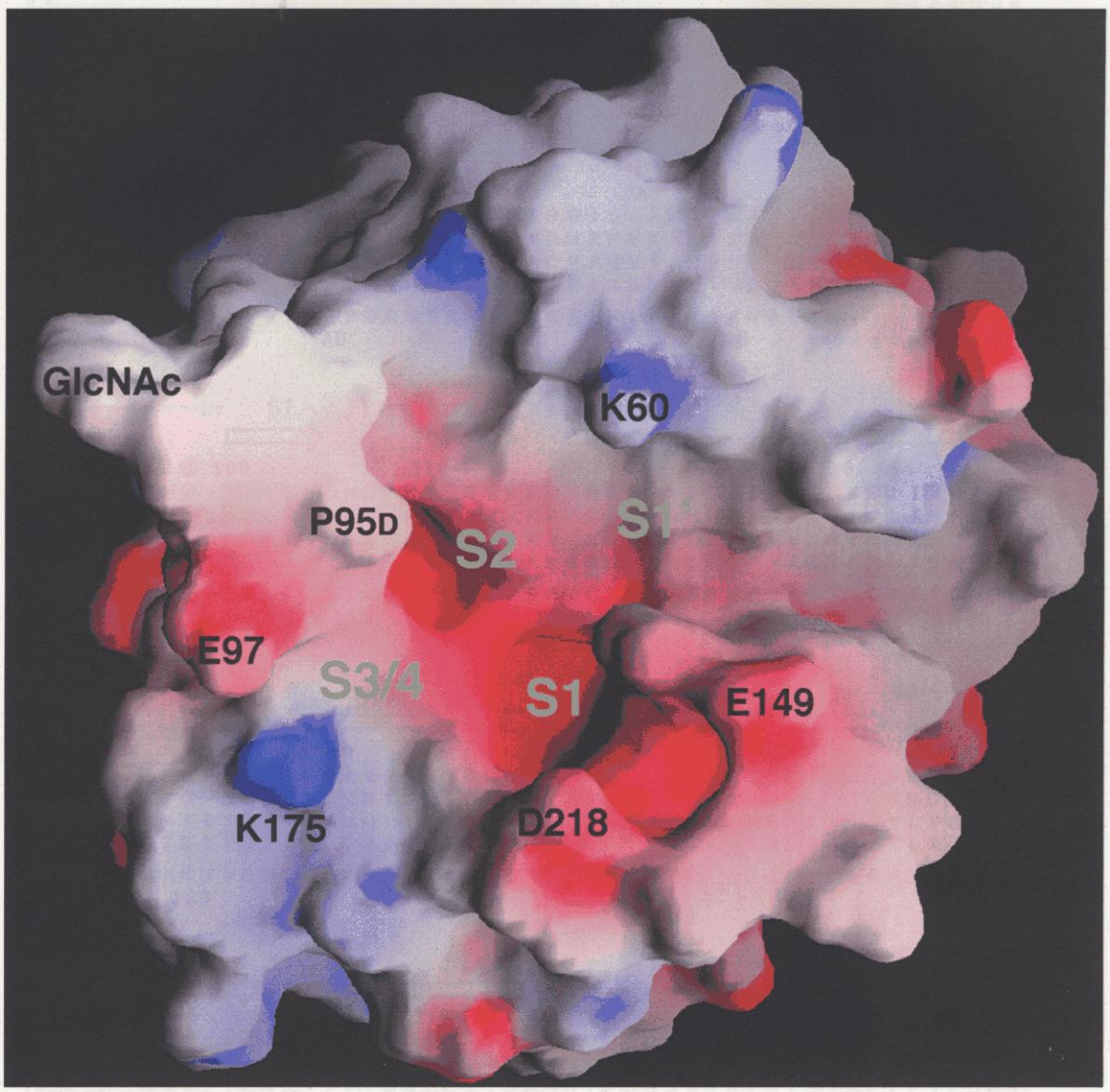

Figure 2-2-2 Overall Structure of Neuropsin (Molecular Surface Diagram) This diagram views from nearly the same direction of Figure 2-2-1. Surface electrostatic potentials was calculated and rendered with the program GRASP (Nicholls *et al.*, 1991; negative potentials are in red and positive in blue). The S1-S4 and S1' sites and characteristic surface residues are labeled.

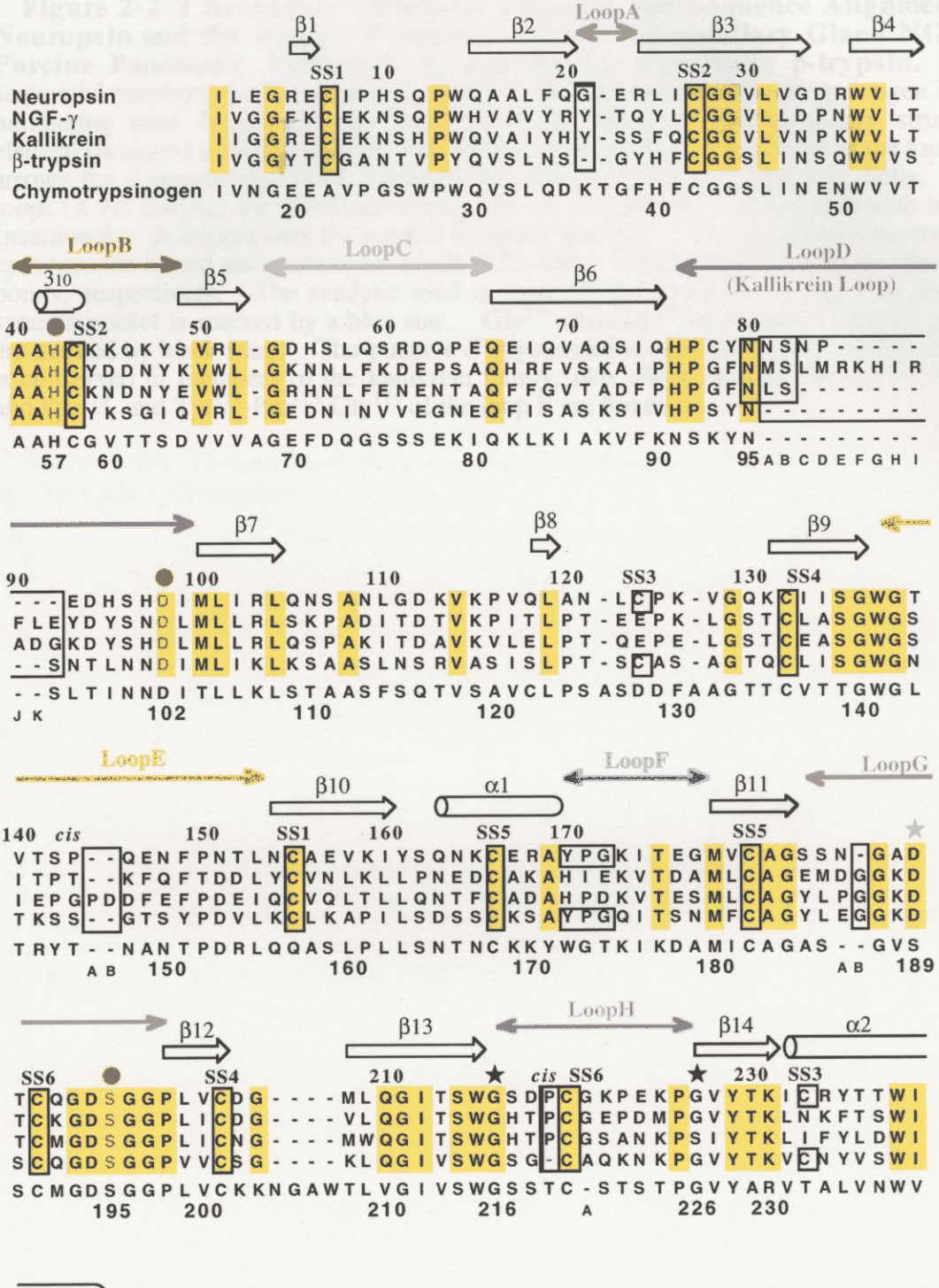
β1
β2
LoopA
β3
β4
SS1
SS2
Neuropsin
NGF-γ
Kallikrein
β-trypsin
Chymotrypsinogen
LoopB
LoopC
LoopD
(Kallikrein Loop)
310
β5
β6
β7
β8
β9
SS3
SS4
LoopE
LoopF
LoopG
β10
α1
β11
cis
SS5
SS6
β12
β13
LoopH
β14
α2

(continued)

Figure 2-2-3 Secondary Structural Elements and Sequence Alignment of Neuropsin and the Related Proteases, Mouse Submaxillary Gland NGF-γ, Porcine Pancreatic Kallikrein A, and Bovine Pancreatic β-trypsin. The sequential numbering of neuropsin is shown at the top, and the chymotrypsinogen based numbering used throughout this paper is at the bottom. The secondary structural element (assigned with the program PROCHECK) of neuropsin are shown at the top with arrows for β-strands (β1-β14), cylinders for α-helices (α1, α2) and a 3_{10}-helix. The loops (A-H) forming the substrate-binding site are marked with colored bars with labels. Insertional or deletional sites are marked by heavy line box. The disulfide-bond-forming cysteines are boxed and marked by labels (SS1-SS6), which correspond to six disulfide-bonds, respectively. The catalytic triad is marked by red circles. Asp^{189} in the S1-specific pocket is marked by a blue star. Gly^{216} and Gly^{226} of the rim of the S1 pocket are marked by black stars. The putative *N*-glycosylation sequence of Asn-X-Ser, which is conserved in members of the kallikrein family, two *cis*-prolines of neuropsin, Pro^{147} and Pro^{219}, and Tyr^{172}-Pro^{173}-Gly^{174} of the loop F are boxed.

Table 2-2-1 Comparison between the Main Chain of Neuropsin and Those of the Other Proteases

Compared Protease	r.m.s. Deviation (Å)
NGF-γ	1.43
β-trypsin	1.26
Kallikrein	1.84

The geometrical differences between main chain atoms of neuropsin and those of each protease except deletion and insertion are shown with r.m.s. deviations. These r.m.s. deviations were calculated with the program LSQKAB.

a

Compared Protease	r.m.s. Deviation (Å)
NGF-γ	0.243
β-trypsin	0.201
Kallikrein	0.200

b

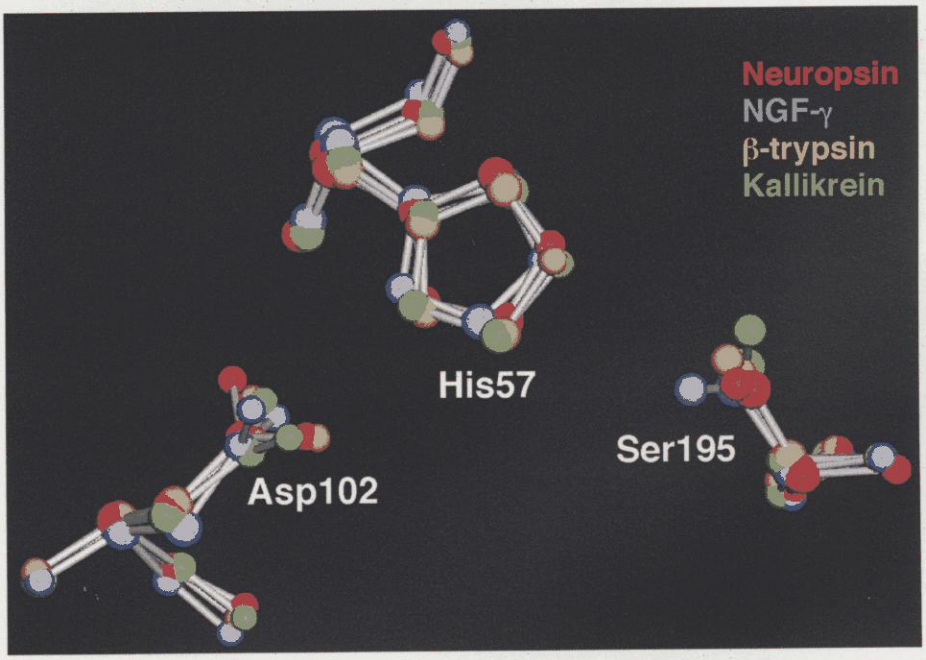

Figure 2-2-4 Comparison between the Catalytic Triad of Neuropsin and Those of the Other Proteases *a*, The geometrical differences between the catalytic triad of neuropsin and that of each protease are shown with r.m.s. deviations. These r.m.s. deviations were calculated with the program LSQKAB. The geometry of the catalytic triad for neuropsin is highly similar to those of the serine proteases with r.m.s. deviations in a range of 0.2-0.25 Å. *b*, The catalytic triads of neuropsin (red), NGF-γ (blue), β-trypsin (yellow), and Kallikrein (green) were superimposed. This diagram was drawn with the program QUANTA.

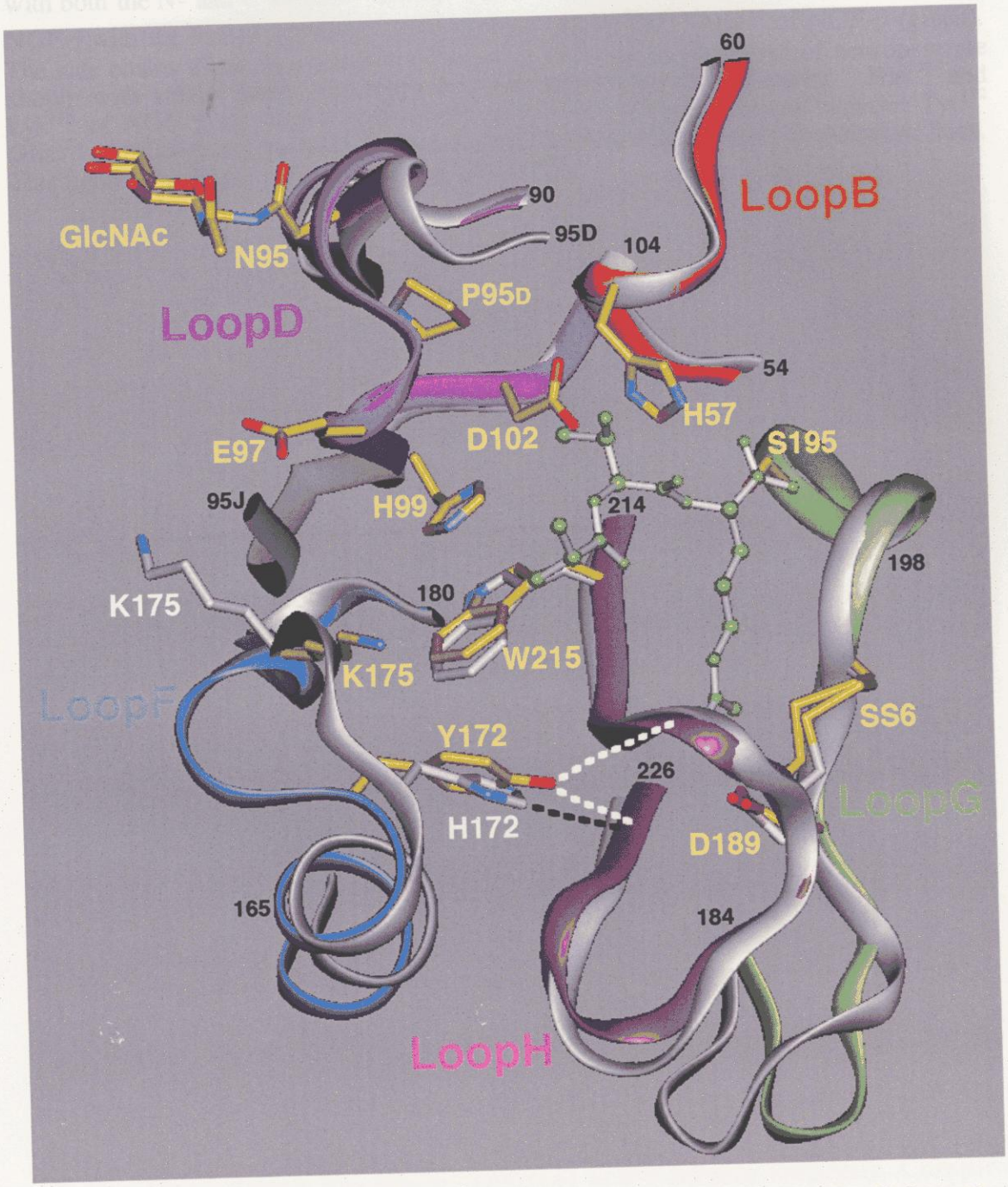

Figure 2-2-5 Comparison of the Surface Loops Forming the Substrate-binding Site between Neuropsin (colored) and NGF-γ-NGF-β in 7S NGF Complex (gray).
(continued)

The C_α-trace of the loop B, D, and F-H of neuropsin are colored as in Figure 2-2-1 with both the N- and C-terminal residue numbers in black and superimposed on those of NGF-γ with the bound substrate, the C-terminal Ala^{116}-Thr^{117}-Arg^{118} of NGF-β (green). The side chains of the key residues of the loops and the catalytic triad of neuropsin are shown with yellow labels, but the others are not shown for the clarity. His^{172} and Lys^{175} of NGF-γ are shown with white label. The hydrogen bonds between Tyr^{172} (His^{172} of NGF-γ) and the loop H are indicated by white (black for NGF-γ) broken lines. This figure was drawn with the program QUANTA.

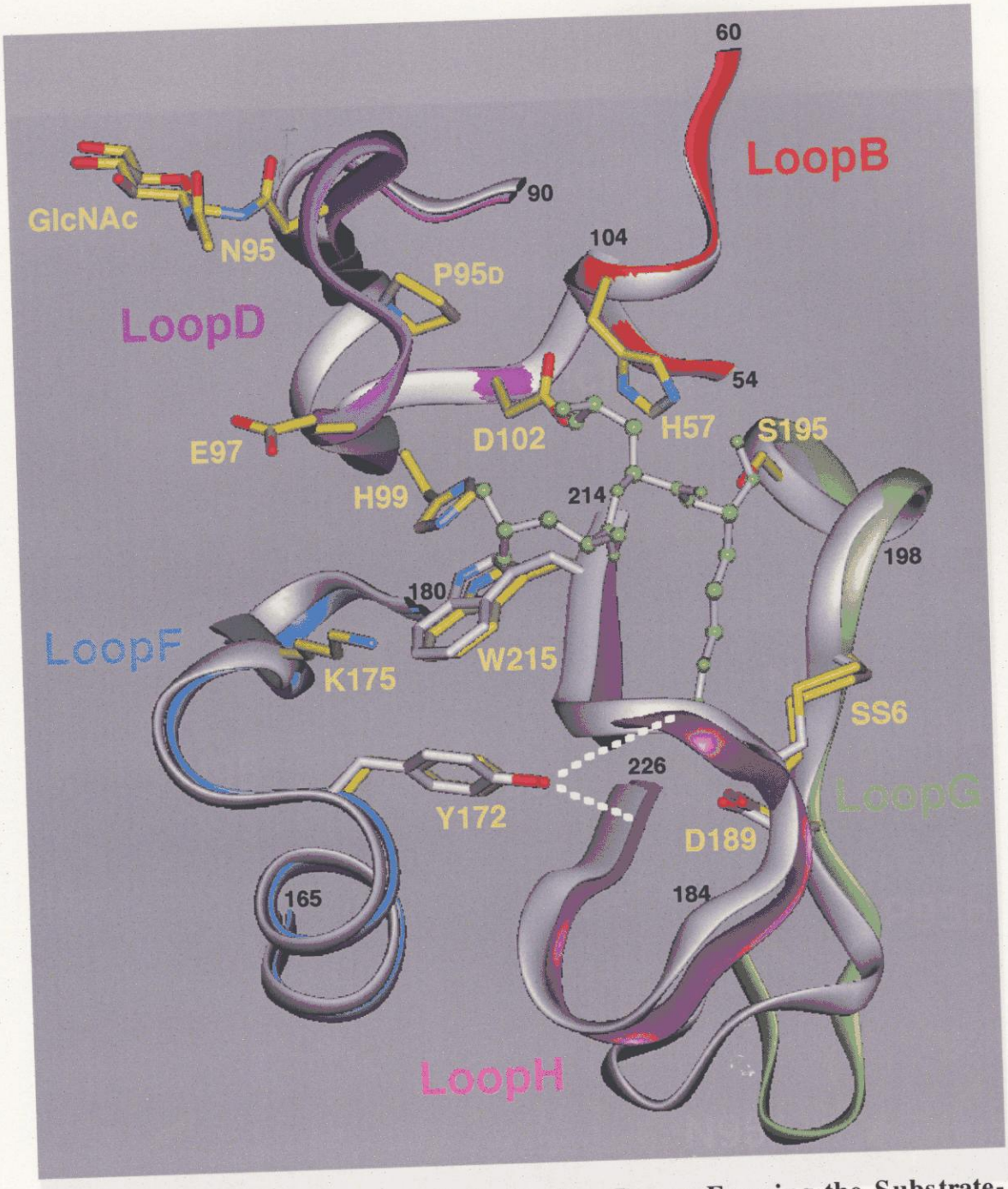

Figure 2-2-6 Comparison of the Surface Loops Forming the Substrate-binding Site between Neuropsin (colored) and β-trypsin-leupeptin Complex (gray). The C_α-trace of the loop B, D, and F-H of neuropsin are colored as in Figure 2-2-1 with both the N- and C-terminal residue numbers in black and superimposed on those of β-trypsin with the bound inhibitor, leupeptin (green) (PDB code: *1JRS*; Kurinov and Harrison, 1996). Labels are as in Figure 2-2-5.

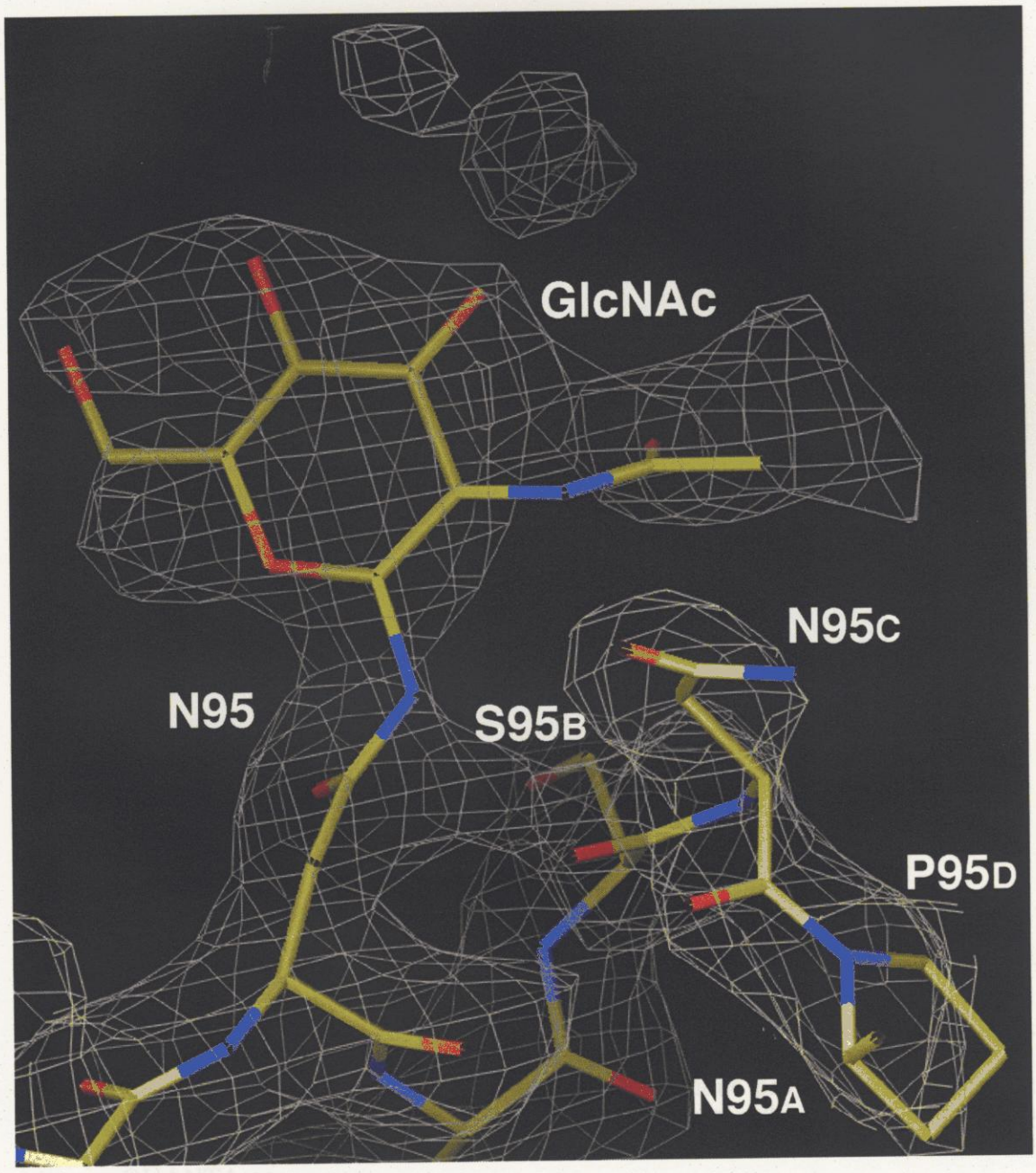

Figure 2-2-7 A $2F_o$-F_c Map nearby the *N*-glycosylation Site (Asn^{95}) A GlcNAc projects to the opposite direction toward the active site (below in this figure). Excessive electron densities are near the GlcNAc residue. These densities are estimated to derive from next sugar. This figure was drawn with the program O.

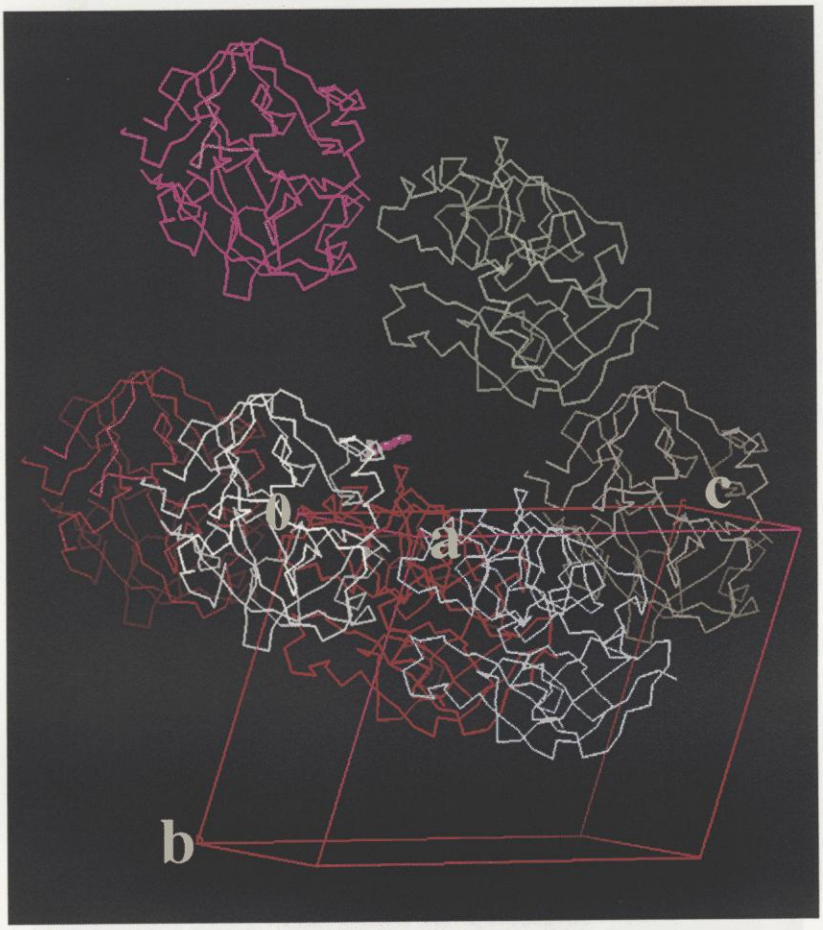

Figure 2-2-8 Crystal Packing of Crystal Form II near the *N*-glycosylated D Loop. Neuropsin molecules are shown with the C_α-trace. A unit cell is drawn with red lines. Three axes (*a*, *b*, and *c*) and the origin (0) are shown with yellow labels. A GlcNAc residue was possessed the white molecule (on the origin), which is surrounded the other molecules, is shown as purple stick. The residue projects to the opposite direction toward the active site that is large solvent space, which shows that more oligosaccharide can add to this glycosylation site. This figure was drawn with the program QUANTA.

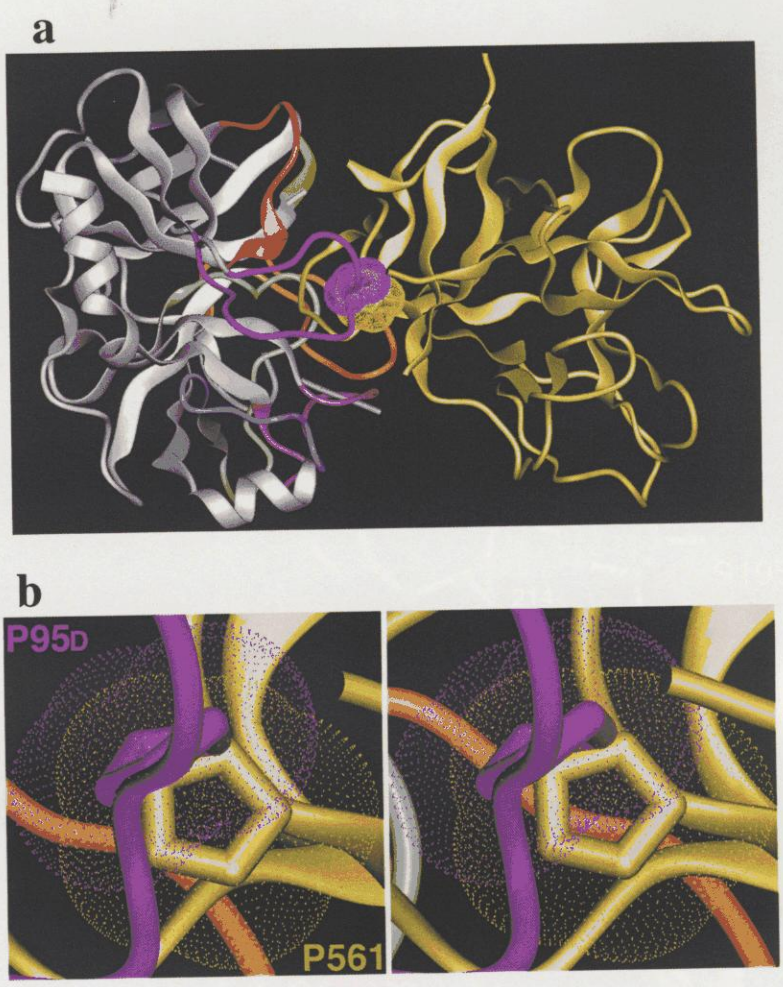

Figure 2-2-9 A Model of Neuropsin and STI complex This complex model was made using coordinate of neuropsin and that of STI complexed with porcine pancreatic β-trypsin. This figures were drawn with the program QUANTA. *a*, Overall structure of neuropsin (colored as in Figure 2-2-1) and STI (yellow) complex. This model reveals steric crashes between the kallikrein loop of neuropsin and the two loops of STI facing toward neuropsin. The van der Waals surfaces of Pro^{95D} of neuropsin and Pro^{561} of STI are shown with dot-surface representations, showing one of the steric crashes in this model. *b*, A stereo diagram of the steric crashed site.

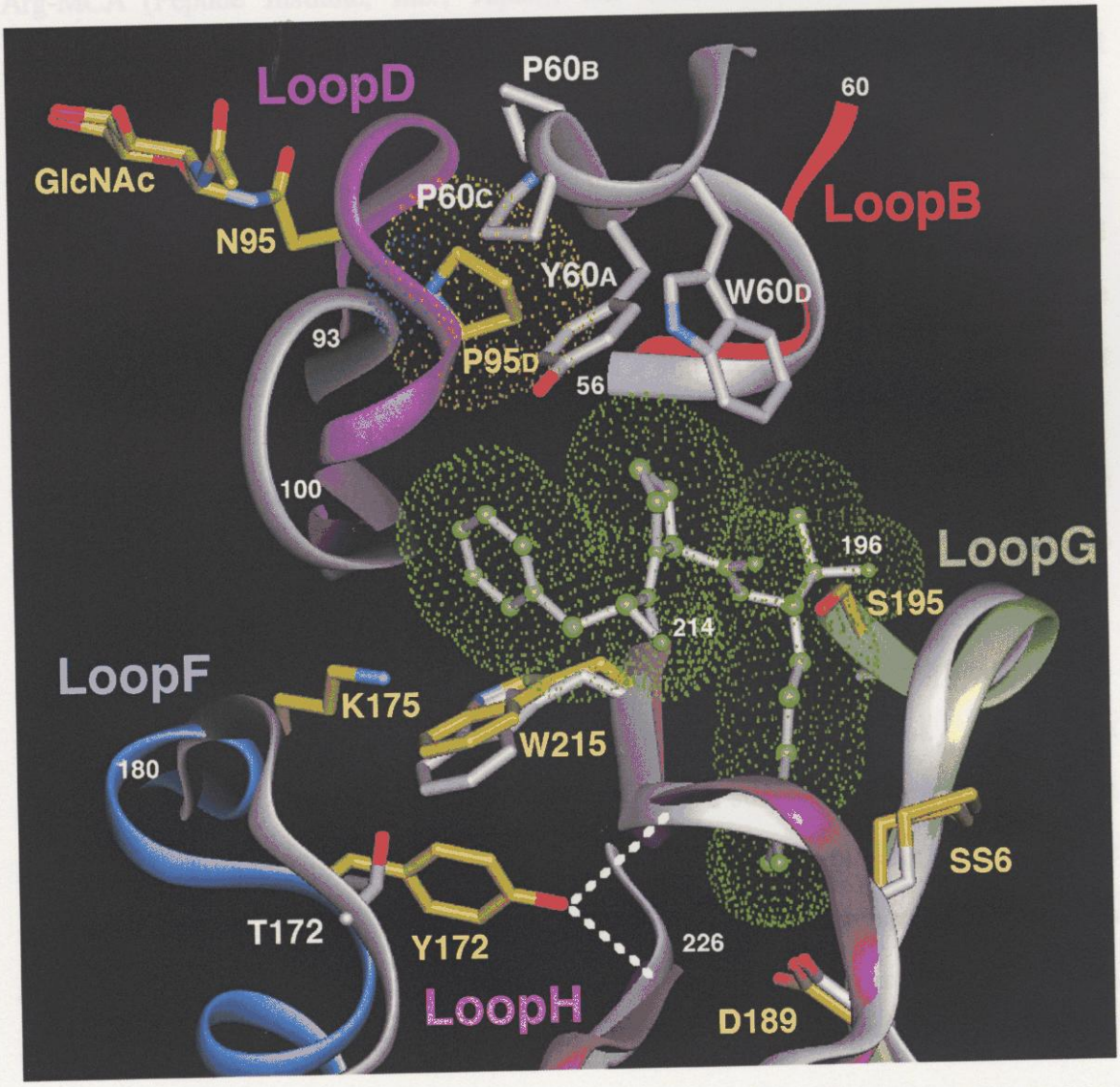

Figure 2-2-10 Comparison of the Surface Loops Forming the S2 Site between Neuropsin (colored) and α-thrombin-D-Phe-Pro-Arg-chloromethylketon Complex (gray). The C_α-traces of the loops of neuropsin, colored as in Figure 2-2-1, are superimposed on α-thrombin complexed with D-Phe-Pro-Arg-chloromethylketon (green). The van der Waals surfaces of the inhibitor peptide and Pro^{95D} of neuropsin are shown with dot-surface representations. Labels are as in Figure 2-2-5. This figure was drawn with the program QUANTA.

2-3. DISCUSSION

A tripeptide substrate preferred for thrombin, *t*-butyloxycarbonyl (Boc) -Val-Pro-Arg-MCA (Peptide Institute, Inc., Japan), has been found to exhibit the highest sensitivity for neuropsin to date (Shimizu *et al.*, 1998). However, poor structural homology between neuropsin and thrombin is evident from the large r.m.s. deviation of 2.7 Å for 78 identical residues. Moreover, thrombin cleaves Boc-Val-Pro-Arg-MCA much faster (33-fold) than Boc-Phe-Ser-Arg-MCA, which is one of the preferred substrates of β-trypsin, whereas the activities of neuropsin for these substrates are comparable. In addition, thrombin also exhibits a significant preference for arginine at the P1 position, but no such preference was observed for neuropsin, as described above. These results, together with structural differences of several loops, verify the unique substrate specificity of neuropsin, even if the P2 preference for proline is analogous to thrombin.

Compared with the subsite preferences on the N-terminal side of the scissile bond, little is known about subsite preferences on the C-terminal side at present. However, a shallow bowl formed by Cys^{42}, Ile^{41}, and Leu^{40} of β-strand β3 seems to provide a hydrophobic S1' site (Figure 2-2-2). The shape of the substrate-binding surface and the surface electrostatic distribution of neuropsin display several differences in details from other serine proteases. One of the pronounced characteristics is the rim of the S1 pocket, where acidic residues, Asp^{218} and Glu^{149}, expose the side chains to the solvent region. Glu^{97} of the kallikrein loop also is projected from the surface. These characteristics may be related to the specificity that are distinct from those of other proteases. Neuropsin exhibits weak proteolytic activities against gelatin and collagen but effectively cleaves fibronectin, as already mentioned. By changing the extracellular environment, neuropsin may exert its limbic effects.

It is an interesting question whether neuropsin could process NGF-β precursor and form 7S NGF complex instead of NGF-γ. In 7S NGF complex, the active site of NGF-

γ was occupied by the C-terminal Arg^{118} of mature NGF-β, as a cleaved product, with extensive interactions of the large nicked kallikrein loop with the C-terminal regions and β-strand of NGF-β. Docking studies suggest that neuropsin would lose most of these interactions although the smaller residues, Thr^{117} and Ala^{116}, of NGF-β could fit to the S2 and S3 sites of neuropsin. In addition, the small cavity of NGF-γ for Ala^{116} of NGF-β is missing in neuropsin. Moreover, Lys^{192}, which is located at the rim of the active site of NGF-γ and forms hydrogen bonds to main chain carbonyls of Thr^{117} and Lys^{74} of NGF-β, is replaced by Gln^{192} in neuropsin. In 7S NGF complex, two zinc ion were located at the interface between NGF-β and NGF-γ to stabilize the complex (Bax *et al.*, 1997). This coordination is also lost when NGF-γ is replaced by neuropsin because zinc-coordinated His^{217} and Glu^{222} in NGF-γ are replaced by Ser^{217} and Lys^{221} in neuropsin. Taken together, these results suggest that neuropsin is incapable of forming 7S NGF complex, even if neuropsin could process NGF-β precursor. However, this will require further investigation.

In addition to neuropsin, three other serine proteases have been reported to be more highly expressed in the central nervous system than in most peripheral tissues. These include myelencephalon specific protease (MSP) (Scarisbrick *et al.*, 1997), neurosin (Yamashiro *et al.*, 1997), and neurotrypsin (Gschwend *et al.*, 1997). MSP and neurosin exhibit sequence identities to neuropsin of 48 and 46%, respectively. Neurotrypsin, which is a multidomain serine protease whose expression is most prominent in the cerebral cortex, the hippocampus, and the amygdala, has a protease domain exhibiting 33% sequence identity to neuropsin. Sequence alignments with neuropsin indicate that these proteases would have different structures of surface loops surrounding the substrate-binding site. Remarkably, the loop D of either of these proteases has no *N*-glycosylation site and no inserted residues. This lack of a kallikrein loop would result in their P2 specificities differing from that of neuropsin. Moreover, the loop G of MSP and of neurosin have no one-residue deletion, which causes

significant structural changes of the loops G and H forming the S1 pocket. Alternatively, compared with neuropsin, neurotrypsin has a three-residue insertion in the loop G and a one-residue deletion in the loop H. These differences would endow these other proteases with substrate specificities different from that of neuropsin.

In conclusion, many aspects of neuropsin structure and function reveal that this hippocampal serine protease displays chimeric structural features of β-trypsin and NGF-γ with novel substrate specificity. These findings could give a clue to the structure-based drug design useful in treatment of pathological conditions such as epilepsy and also useful in analyzing the processes of synaptic plasticity.

3. IDENTIFICATION, PURIFICATION, AND CHARACTERIZATION OF A SPECIFIC INHIBITOR FOR NEUROPSIN

3-1. MATERIALS AND METHODS

Preparation of Neuropsin and Its Antibodies

Recombinant neuropsin was produced as pro-type in cultured medium using a baculovirus expression system and purified as described previously (see *2-1. MATERIALS AND METHODS*). The pro-type neuropsin was activated by treating at 37℃ for 50 min with lysyl endopeptidase (EC 3.4.21.50; Wako Pure Chemical Industries, Ltd., Japan) coupled to Sepharose 4B gel (Amersham Pharmacia Biotech, UK). Proteolytic activity of the activated neuropsin was determined with a synthetic chromogenic substrate, Boc-Val-Pro-Arg-MCA (Peptide Institute, Inc., Japan) (Shimizu *et al.*, 1998). Neuropsin cDNA and the mutant cDNAs (DS211VA, D206V, and C7S), in the pED1 vector containing the cytomegalovirus enhancer and chicken β-actin promoter (Niwa *et al.*, 1991; Mizuguchi *et al.*, 1996), were constructed (Oka *et al.*, in preparation) and transfected into neuro2a cells (Institute for Fermentation, Japan). The amount of recombinant neuropsin and the mutants in the cultured-supernatant was determined based on bands density stained using a CBB G-250-based protein staining reagent, GELCODE CBB reagent (Pierce Chemical Co., USA), followed by 10% SDS-PAGE. Purified recombinant neuropsin (baculo) was used as a control of the amount. Rat anti-neuropsin monoclonal antibodies (mAb), F12mAb and B5mAb, (Medical & Biological Laboratories Co., Ltd., Japan) (Momota *et al.*, 1998) and rat immunoglobulin G (IgG; ICN Pharmaceuticals, Inc., USA) coupled to Affi-Gel Hz gel (Bio-Rad Laboratories, USA) or rabbit anti-neuropsin polyclonal antibody (pAb), #11pAb, were used for immuno-precipitation and affinity purification of specific inhibitors for neuropsin or for western blot analysis, respectively.

Fractionation of Mouse Brain Homogenate

The hippocampus and cerebral cortex were took out from adult mice (10 weeks old, Slc: ddY, Japan SLC, Japan) and the tissues were mixed and homogenized using a

Dounce homogenizer with 1 ml of ice-cold 20 mM Tris (hydroxymethyl) aminomethane (Tris)-HCl buffer (pH 7.4) containing 0.15 M NaCl for the tissues recovered from one mouse. After incubation on ice for 30 min and centrifugation at 10,000 x g at 4℃ for 10 min, the soluble fraction was recovered (0.15 M NaCl-soluble fraction). The sediment was resuspended with an equal volume of ice-cold 20 mM Tris-HCl buffer (pH 7.4) containing 2% *t*-octylphenoxy-polyethoxyethanol (Triton X-100), homogenized, and stood on ice for 30 min. After centrifugation at 102,000 x g at 4℃ for 10 min, a first Triton-soluble fraction was recovered (first Triton-soluble fraction). The first Triton-insoluble residue was pelleted, resuspended with an equal volume of ice-cold 20 mM Tris-HCl buffer (pH 7.4) containing 1% Triton X-100, homogenized, and stood on ice for 30 min. After further centrifugation at 208,000 x g at 4℃ for 10 min, a second Triton-soluble fraction was recovered (second Triton-soluble fraction). The second Triton-insoluble residue was homogenized in an equal volume of ice-cold 20 mM Tris-HCl buffer (pH 7.4) containing 0.5 M NaCl, incubated on ice for 30 min, then centrifuged at 383,000 x g at 4℃ for 10 min. Finally, the supernatant was recovered as a cytoskeleton-rich fraction (Tohyama *et al.*, 1994; Shimizu *et al.*, 1998). The protein contents were determined with bicinchoninic acid (BCA) protein assay reagent (Pierce Chemical Co., USA) and albumin standard (Pierce Chemical Co., USA).

Detection of Protease Inhibitors for Neuropsin

Each fraction including 3 mg of protein was incubated with 2 μg of recombinant neuropsin (baculo) on ice for 1 hour and rotated in the presence of rat IgG (more than 20 μg of IgG / 2 μg recombinant neuropsin (baculo)) coupled to Affi-Gel Hz gel at 4℃ for 30 min for the purpose of pre-cleaning. After brief centrifugation, the supernatant was mixed with F12mAb (more than 20 μg of IgG) coupled to Affi-Gel Hz gel in 20 mM Tris-HCl (pH 7.5) buffer containing 0.15 M NaCl and rotated at 4℃ for 15 hours. The gel was washed with 20 mM Tris-HCl buffer (pH 7.5) containing 0.15 M NaCl, mixed with

an equal volume of 5 x SDS-PAGE gel loading buffer containing 0.3 M Tris-HCl (pH 6.8), 10% sodium dodecyl sulfate (SDS), 25% glycerol, 0.025% bromophenol blue (BPB), and 100 mM dithiothreitol (DTT) boiled for 5 min, and subjected to 5-15% SDS-PAGE (Laemmli, 1970). The proteins were transferred to polyvinylidene difluoride (PVDF) membrane (Bio-Rad Laboratories, USA). After blocking with 0.1M Tris-HCl buffer (pH 7.5) containing 0.15M NaCl and 0.1% polyoxyethylene (20) sorbitan monolaurate (Tween 20) (TTBS) with 5% skim milk for 30 min at room temperature, the membranes were reacted with #11pAb and then anti-rabbit IgG conjugated with alkaline phosphatase (AP) (Bio-Rad Laboratories, USA) in TTBS buffer containing 5% skim milk. The secondary antibody was detected by enhanced chemiluminescence, Immun-Star Substrate (Bio-Rad Laboratories, USA). After development, the band intensities were evaluated with the program Quantity One (Toyobo Co., Ltd., Japan)

Isolation of 65-kDa Complex

Triton-soluble fraction (430 mg of protein) was incubated with activated recombinant neuropsin (baculo) on ice for 1 hour and rotated in the presence of rat IgG coupled to Affi-Gel Hz gel at 4℃ for 30 min. After brief centrifugation, the supernatant was mixed with F12mAb coupled to Affi-Gel Hz gel, rotated, and washed sequentially based on the above immunoprecipitation. The ratio of protein was activated recombinant neuropsin (baculo): Triton-soluble fractions: F12mAb = 1: 7,600: 10 (wt./wt./wt.). The Affi-Gel Hz gel was packed into an open column, Sepacol Mini (Seikagaku Corporation, Japan). The packed gel was washed with five bed volumes of 20 mM Tris-HCl buffer (pH 7.5) containing 0.15 M NaCl and then washed with five bed volumes of 20 mM Tris-HCl buffer (pH 7.5) containing 0.5 M NaCl. The 65-kDa complex was eluted with 0.2 M Glycine-HCl buffer (pH 2.5) and then the eluted solution was neutralized with 1 M Tris-HCl (pH 8.0). After dialysis with 2,000-fold volume of 20 mM Tris-HCl buffer (pH 7.5) containing 0.15M NaCl, 0.5 mM DTT, and 1 mM

phenylmethylsulfonyl fluoride (PMSF) at 4℃ for 2.5 hours, the sample was freeze-dried overnight.

Peptide Sequence Determination

The freeze-dried sample was resuspended with distilled water, subjected to 10% SDS-PAGE, and stained with CBB R-250. A 65-kDa band was excised, and digested with 3 μg/ml of *Achromobacter lyticus* protease I (API) (Masaki *et al.*, 1981; Kawasaki *et al.*, 1990) in 50 mM Tris-HCl buffer (pH 9.0) containing 1 mM ethylenediamine-N,N,N',N'-tetraacetic acid (EDTA) and 0.1% SDS at 37℃ overnight. The digests were separated using an HPLC, model 1100 liquid chromatography system (Hewlett-Packard Co., USA) on a DEAE-5PW (1 x 20 mm; Tosoh, Japan) and a CAPCELL PAK RP18 (1 x 100 mm; Shiseido, Japan), which were linked tandemly, with a linear gradient of 0-48% acetonitrile containing 0.1% trifluoroacetic acid (TFA) for 96 min. Fractionated peptides were subjected to protein sequencing and mass spectrometry as described previously (Masutani *et al.*, 1999).

SPI3 and Neuropsin Kinetics

Recombinant Serine Proteinase Inhibitor 3 (SPI3) was prepared with the *Pichia pastoris* expression system (Sun *et al.*, 1995a). To obtain an SDS-stable complex of recombinant SPI3 and activated recombinant neuropsin (baculo), 200 ng of recombinant SPI3 was added to 100 ng of activated recombinant neuropsin (baculo) and incubated at 37℃ for 20 min. Samples containing either recombinant SPI3 and activated recombinant neuropsin (baculo) alone were incubated in parallel. Three identical sample sets were separated by reducing 12.5% SDS-PAGE. One set was silver-stained, and the other two sets were transferred to nitrocellulose membrane and immunoblotted with either #11pAb or rabbit anti-SPI3 antibody.

Also, the association rate constant between recombinant SPI3 and activated recombinant neuropsin (baculo) were determined. A constant amount of activated recombinant neuropsin (baculo) (0.2 nM) was mixed with different concentrations of recombinant SPI3 and excess substrate (40 mM Boc-Val-Pro-Arg-MCA) in a final volume of 200 μl in 20 mM Tris-HCl buffer (pH 7.4) containing 150 mM NaCl and 0.1% PEG 8000. The reactions were monitored at 37℃ for 2 hours with a spectrofluorometer, LS50B (Perkin-Elmer Co., USA) using an excitation wavelength of 370 nm and an emission wavelength of 450 nm, determining residual activity periodically. The interactions of recombinant SPI3 with activated recombinant neuropsin (baculo) were determined with the progress curve method followed by slow binding inhibition kinetics (Morrison and Walsh, 1988).

$$P = v_s t + \frac{(v_z - v_s)(1 - e^{-k_{obs}t})}{k_{obs}}$$

where P is the concentration of product at time t, k_{obs} is the apparent first order rate constant, and v_z and v_s are the initial and steady state velocities, respectively. The association constant (k_{ass}) was calculated using the following equation.

$$k_{ass} = k_{obs}\left(1 + \frac{[S]}{K_m}\right)$$

[S] is the concentration of substrate and K_m is the Michaelis-Menten constant. K_i is essentially obtained by the Guy Salvesen and Hideaki Nagase method (Salvesen and Nagase, 1989).

$$K_i = \frac{K_{i(app)}}{1 + \frac{[S]}{K_m}} \qquad \left(\frac{v_0}{v_i} = 1 + \frac{[I]}{K_{i(app)}} \right)$$

v_0 is the enzyme-catalyzed hydrolysis rate in the absence of an inhibitor. v_i is the inhibited rate. Values were determined from Dixon plots. In the present study, K_m, k_{cat}, and k_{cat} / K_m of activated recombinant neuropsin (baculo) were 123.6 μM, 4.2 s^{-1}, and 33980 $M^{-1}s^{-1}$, respectively.

In Situ Hybridization of SPI3

For preparation of riboprobes, the SPI3 target sequence was amplified with a single cDNA synthesized from the hippocampal total RNA by one round of polymerase chain reaction (PCR) using primers 5'-CCAAAGTTTAAGCTGGAGGAGAA-3' / 5'-CTGAC-AGGAATACCCTTTGCTCA-3' (338 base pairs (bp): 887-1224 bp; Figure 3-2-5), and the PCR fragment was subcloned in pGEM-T easy vector (Figure 3-1-1; Promega Co., USA). [^{35}S]-labeled riboprobes were prepared according to the manufacturer's instructions (Roche Diagnostics, Germany): antisense, Nco I (Takara Shuzo Co., Ltd., Japan) and SP6 RNA polymerase (Roche Diagnostics, Germany); sense, Sal I (Takara Shuzo Co., Ltd., Japan) and T7 RNA polymerase (Roche Diagnostics, Germany). *In situ* hybridization histochemistry was performed as previously described (Chen *et al.*, 1995). To determine brain areas labeled with SPI3 and neuropsin (B41) (Chen *et al.*, 1995) riboprobes, 14-μm thick coronal sections were sliced from fresh frozen brains (8 weeks Slc: ddY) on a cryostat and thaw-mounted onto slides coated with 0.1% 3-aminopropyltriethoxy silane in acetone. No signals were detected on the adjacent sections incubated in control hybridization mixture containing sense probe (Figure. 3-2-6b).

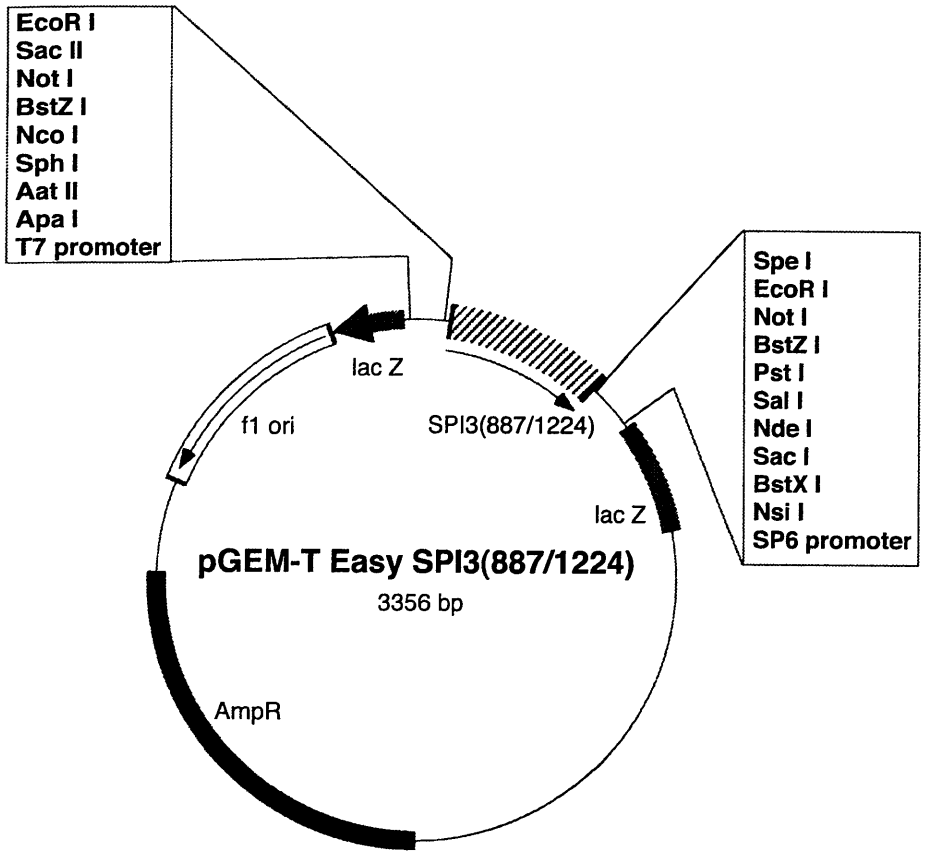

Figure 3-1-1 A Plasmid Map of pGEM-T Easy SPI3(887/1224) This plasmid has a fragment of SPI3 gene (The GenBank accession: *MMU25844*, The National Center for Biotechnology Information (NCBI); *http:// www.ncbi.nlm.nih.gov/ Genbank/GenbankOverview.html*) from 887 to 1224 (338 bp) in multiple cloning site (MCS). Open boxes show restriction sites near MCS. *AmpR*, *f1 ori*, and *lacZ* show the β-lactamase (an ampicillin resistant gene) coding region, the origin of replication of the filamentous phage f1, and the α-peptide coding regions of the enzyme β-galactosidase, respectively.

3-2. RESULTS

Detection of Neuropsin-binding Proteins in Fractions

I screened for neuropsin-specific inhibitors present in adult mouse brain *in vivo*. I monitored whether recombinant neuropsin (baculo), originating from the baculovirus expression system, formed SDS-stable complexes with molecules within extracts prepared from adult mouse hippocampi and cerebral cortices, in which neuropsin mRNA is expressed most abundantly (Chen *et al.*, 1995). The tissues were homogenized and fractionated into 0.15 M NaCl-soluble, Triton-soluble (first and second), and cytoskeleton-rich (0.5 M NaCl-soluble) fractions as described in *3-1. MATERIALS AND METHODS*. As shown in Figure 3-2-1a, the 65-kDa complex was detected in all fractions with both activated and pro-type neuropsin (baculo), while the 230-kDa complex was detected in the 0.15 M NaCl fraction with activated recombinant neuropsin (baculo), but not with pro-type recombinant neuropsin (baculo). When a large amount of each fraction was immunoprecipitated with anti-neuropsin antibody and subjected to 10% SDS-PAGE and western blotting (Figure 3-2-1b), the endogenous brain neuropsin and 65-kDa complex were also existed in the 0.15 M NaCl- and Triton-soluble fraction, respectively. It suggests that the 65-kDa complex is obtained from the endogenous neuropsin and the target molecule.

To investigate which residue on neuropsin is related to the formation of the SDS-stable 65-kDa complex, I prepared activated recombinant neuropsin (neuro2a) proteins, wild type and the mutants with disruptions of protease active pocket without proteolytic activity; DS211VA and D206V, and of cysteine residues with proteolytic activity; C7S (Figure 3-2-2a). The protease active pocket mutants (DS211VA and D206V) of activated recombinant neuropsin (neuro2a) did not form the 65-kDa complex, while wild type and C7S mutant of activated recombinant neuropsin (neuro2a) formed the 65-kDa complex (Figure 3-2-2b). It is suggested that the target molecule is a specific inhibitor through the active pocket of neuropsin.

Purification and Identification of 65-kDa complex

Triton-soluble fraction containing activated recombinant neuropsin (baculo) was applied to an F12mAb coupled to Affi-Gel Hz affinity column and the 65-kDa complex was eluted with a 1.58 x 10^3-fold purification and a yield of 33.8% (Table 3-2-1). To determine the target molecule forming 65-kDa complex by micro-sequencing, the eluant was freeze-dried and subjected to 10% SDS-PAGE. A part was, however, degraded after being freeze-dried to a final yield of 1.5%, and the 41-kDa band was appeared (Figure 3-2-3).

Purified 65-kDa complex was subjected to 10% SDS-PAGE, each band (65- and 41-kDa) on gel was digested with API, and peptide sequences were determined using a protein sequencer. Peptide sequencing identified the inhibitor to be serine proteinase inhibitor 3 (SPI3; The Protein Information Resource (PIR) accession: *A57488*, The National Biomedical Research Foundation (NBRF); *http:// www-nbrf.georgetown.edu/ nbrf/index.html*; Figure 3-2-4) for 65-kDa complex and peptide mass chromatography confirmed this identification. Fifty-seven percent of SPI3 was sequenced(Table 3-2-2). In addition, I screened an adult mouse hippocampal cDNA library by PCR with primers based on the peptide sequence obtained from the degraded 65-kDa complex (41-kDa species) which resulted in amplification of the SPI3 cDNA. Thus, it was found that addition of recombinant neuropsin to adult mouse hippocampal and cortical extracts resulted in the appearance of SPI3-neuropsin (65-kDa) complex.

Effect of SPI3 on the Proteolytic Activity of Neuropsin

I investigated whether SPI3 could form an SDS-stable complex with activated recombinant neuropsin (baculo) or inhibit the proteolytic activity of activated recombinant neuropsin (baculo). I purified recombinant SPI3 with a *Pichia pastoris* expression system (Sun *et al.*, 1995b). Addition of recombinant SPI3 to recombinant neuropsin (baculo) resulted in the formation of a 65-kDa complex, which was subjected to reduction,

boiling, and 12.5% SDS-PAGE (Figure 3-2-5). The complex was recognized by antibodies against both neuropsin and SPI3. The association rate constant k_{ass}, for interaction of activated recombinant neuropsin (baculo) with recombinant SPI3, was determined under pseudo first-order conditions using the progress curve method (Morrison and Walsh, 1987). The k_{ass} and K_i for complex formation were calculated as $3.4 \pm 0.22 \times 10^6$ $M^{-1}s^{-1}$ and 0.8 nM, respectively (Figure 3-2-6). These were well within the range for physiologically significant interactions (Potempa *et al.*, 1994).

Localization of SPI3 in the Adult Mouse Brain

I estimated whether neuropsin could co-localize with SPI3 *in vivo*. It has been suggested that SPI3 was not secreted and had an intracellular role in monocytes and granulocytes (Scott *et al.*, 1996; Scott *et al.*, 1999). I, therefore, investigated whether areas of the brain expressing neuropsin mRNA also expressed SPI3 mRNA by *in situ* hybridization histochemistry (Figure 3-2-7). The SPI3 mRNAs were expressed in most equivalent brain areas which the neuropsin mRNAs were expressed. In the hippocampal formation, SPI3 mRNAs were expressed in the CA3 pyramidal neurons very strongly, in the CA1 pyramidal neurons moderately, and in the granule cells of the dentate gyrus weakly, while the CA1-3 subfields but not the dentate gyrus expressed neuropsin mRNAs (Chen *et al.*, 1995). In the frontal cortex, labeled neurons spread to layers V moderately and II and IV weakly, which have similar profiles with those of neuropsin (Chen *et al.*, 1995). Neurons in the cingulate cortex were also labeled moderately and the signal continued posteriorly into the retrosplenial cortex and presubiculum like that of neuropsin mRNA signals (Chen *et al.*, 1995). The anterior olfactory nuclei, medial septal nucleus, diagonal bands, and amygdaloid complex were also labeled as well as with neuropsin probe (Chen *et al.*, 1995). However, in the forebrain limbic area, the lateral septal nucleus was labeled with neuropsin but not SPI3 riboprobe. In contrast,

there were cells positive with intense SPI3 mRNA signals in the thalamus, hypothalamus, and choroid plexus, though no neuropsin-positive signals were found in these areas.

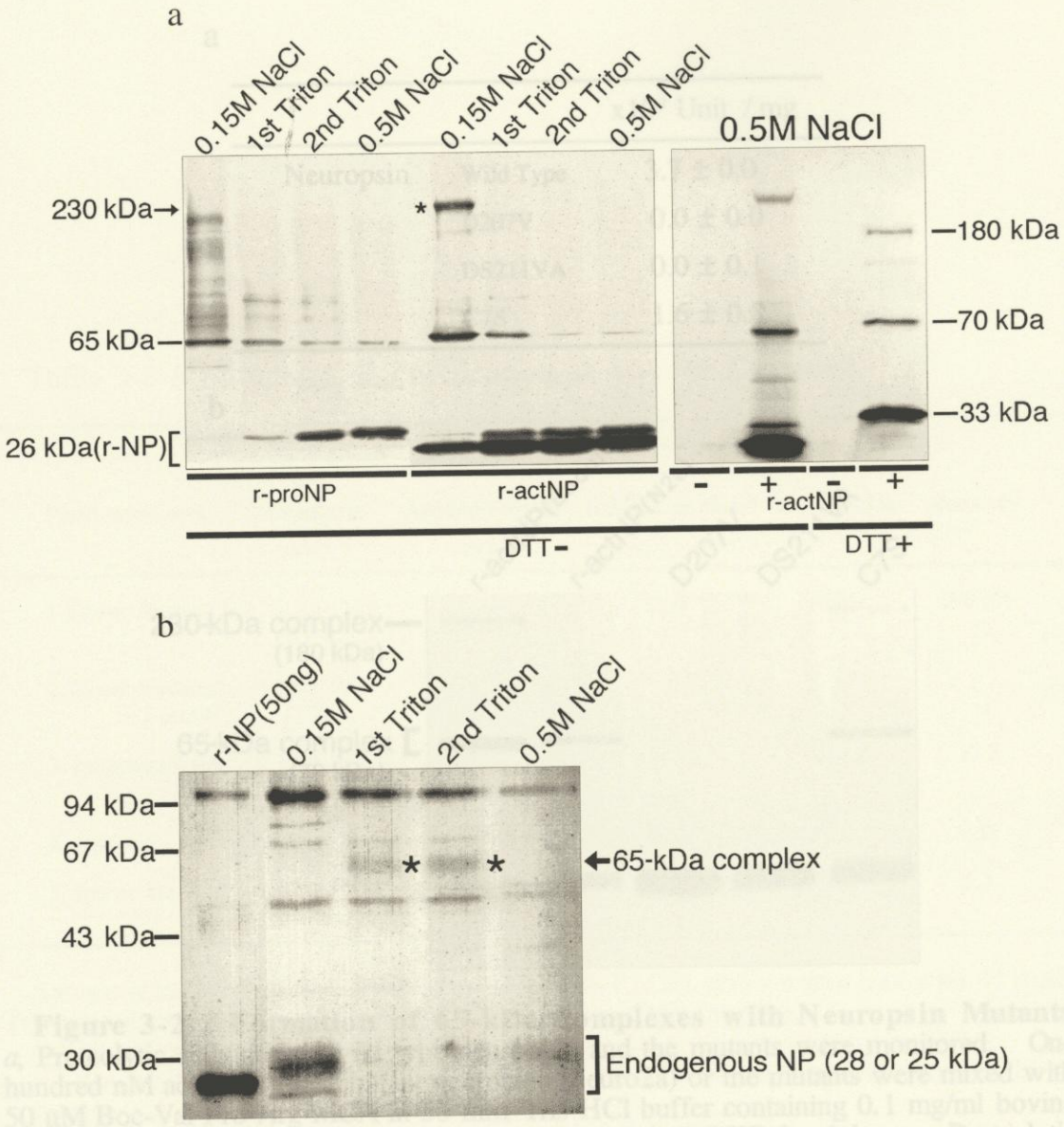

Figure 3-2-1 Detection of SDS-stable Complexes with Neuropsin in Adult Mouse Hippocampal and Cortical Extracts *a*, The hippocampal and cortical tissues were took out and fractionated into a 0.15 M NaCl-soluble fraction, first Triton-soluble fraction, second Triton-soluble fraction, and cytoskeleton-rich fraction (0.5 M NaCl-soluble fraction). Each fraction (3 mg of protein) was mixed with purified activated recombinant neuropsin (baculo) (2 μg), and immunoprecipitated using F12mAb (20 μg) coupled to Affi-Gel Hz beads. Immunoprecipitated samples were subjected to 5-15% SDS-PAGE, followed by western blot with #11pAb. *b*, Each fraction (33 mg of protein) was immunoprecipitated using B5mAb (450 μg) coupled to Affi-Gel Hz beads. A quarter of each precipitant was subjected to 10% SDS-PAGE, followed by western blot with #11pAb. Asterisks are shown as the endogenous 65-kDa complexes. This film was over-exposed relative to Figure 3-2-1a.

a

		x10^{-1} Unit / mg
Neuropsin	Wild Type	3.7 ± 0.0
	D207V	0.0 ± 0.0
	DS211VA	0.0 ± 0.1
	C7S	1.6 ± 0.8

b

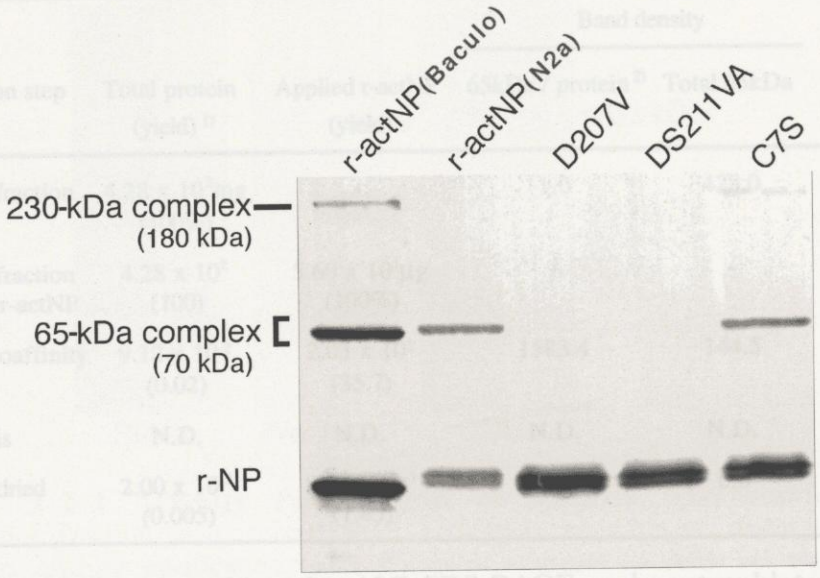

Figure 3-2-2 Formation of 65-kDa Complexes with Neuropsin Mutants
a, Proteolytic activities of wild type neuropsin and the mutants were monitored. One hundred nM activated recombinant neuropsin (neuro2a) or the mutants were mixed with 50 μM Boc-Val-Pro-Arg-MCA in 50 mM Tris-HCl buffer containing 0.1 mg/ml bovine serum albumin (BSA) and 0.02% NaN_3, and incubated 25℃ for 1 hour. Proteolytic activities are shown as Unit (μmol/min)/mg (Oka *et al.*, in preparation). *b*, Each activated recombinant neuropsin (neuro2a) or mutant (0.6 μg) was mixed with 0.15 M NaCl soluble fraction (1.5 mg of protein), immunoprecipitated using F12mAb coupled to Affi-Gel Hz beads, subjected to reducing 10% SDS-PAGE (100 mM DTT), and followed by western blot with #11pAb. These mutants are named on the basis of the nucleotide sequence of neuropsin (Chen *et al.*, 1995). According to numbering of neuropsin amino acid sequence aligned with bovine chymotrypsinogen, D207V, DS211VA, and C7S are replaced from Asp^{189} to Val, from Asp^{194}-Ser^{195} to Val-Ala, from C^{4C} to Ser, respectively. Note that no SDS-stable complexes were formed with two mutants (D206V and DS211VA) which were treated with lysyl endopeptidase coupled to Sepharose 4B gel.

Table 3-2-1 Summary of Purification of 65-kDa Complex

Purification step	Total protein (yield) [1]	Applied r-actNP (yield)	Band density: 65kDa / protein [2]	Band density: Total 65kDa	Recovery
1.Triton fraction	4.28×10^{2}mg (100%)	-	1.0	428.0	100.0%
2.Triton fraction + r-actNP	4.28×10^{2} (100)	5.60×10^{1}µg (100%)	-	-	-
3. Immunoaffinity	9.12×10^{-2} (0.02)	2.03×10^{1} (35.7)	1583.4	144.5	33.8
4. Dialysis	N.D.	N.D.	N.D.	N.D.	N.D.
5. Freeze-dried	2.00×10^{-2} (0.005)	8.14×10^{-1} (1.45)	327.7	6.6	1.5

Sample at each step was subjected to 10% SDS-PAGE, and western blot with #11pAb. The band densities were evaluated with the program Quantity One.

[1] Yield of protein contents

[2] [density of 65-kDa in each step / density of 65-kDa in Triton-soluble fraction] / mg protein

N.D.: not determined.

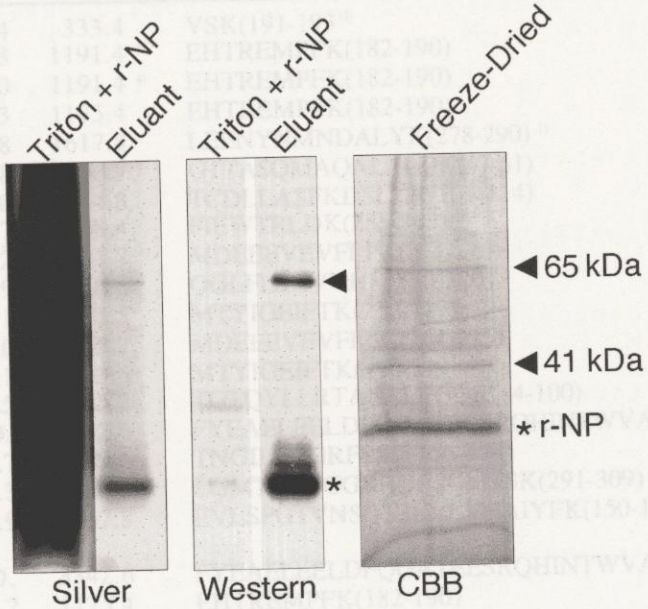

Figure 3-2-3 Affinity Purification of 65-kDa SDS-stable Complex Triton-soluble fraction was mixed with activated recombinant neuropsin (baculo), subjected to affinity purification with F12mAb coupled to Affi-Gel Hz beads, and followed by 10% SDS-PAGE. The 25 μg of protein was applied to Lanes of "Triton + r-NP" (activated recombinant neuropsin (baculo): Triton fraction = 7600:1 [wt./wt.]). The 0.3 μg of protein in eluants for F12mAb immunoaffinity chromatography was applied to Lanes of "Eluant". The 1.2 μg of protein, which was dialyzed, freeze-dried, and resuspended with distilled water, was applied to a lane of "Freeze-Dried". Arrow heads show 65-kDa complex protein, and asterisks show recombinant neuropsin. Note that 65-kDa and 41-kDa bands on the CBB-stained gel were subjected to peptide analysis.

Table 3-2-2 Mass Spectroscopy Analysis of the Peptides from Digested 65-kDa Complex

Peak	M. W. Observed	M. W. Calculated	Predicted peptide
41K-10	333.4	333.4	VSK(191-193)[3]
41K-20	1191.8	1191.4 [4]	EHTREMPFK(182-190)
41K-21	1191.0	1191.4 [4]	EHTREMPFK(182-190)
41K-35	1175.3	1175.4	EHTREMPFK(182-190)
41K-53	1616.8	1617.8	LEENYNMNDALYK(278-290) [1]
41K-64	1506.8	1506.7	GTTASQMAQALALDK(47-61)
	1545.0	1544.8	TCDLLASFKDSCLK(101-114)
41K-65	1207.7	1208.4	FIEWTRLDK(255-263)
41K-68	1482.2	1481.7 [4]	MDEEEVEVFLPK(264-275)
41K-70	1256.9	1256.5	QGLFLSKVVHK(310-320)
41K-74	1203.1	1203.5	MTYIGEIFTK(210-219)
	1466.0	1465.7	MDEEEVEVFLPK(264-275)
41K-75	1204.1	1203.5	MTYIGEIFTK(210-219)
41K-78	1954.5	1955.2	TGTQYLLRTANRLFGDK(84-100)
41K-80	N.D.	3342.6	FYEAELEELDFQGATEESRQHINTWVAK(115-142) [1]
41K-85	1340.7	1399.6	TNGILFCGRFSSP(366-378)
41K-88	1935.3	1936.2	LGMTDAFGGRADFSGMSSK(291-309)
41K-91	2467.9	2467.8	EVLSPGTVNSDTSLVLVNAIYFK(150-172)
65K-96	N.D.	3342.6	FYEAELEELDFQGATEESRQHINTWVAK(115-142)[1]
pooled-65K[2]	1176.2	1175.4	EHTREMPFK(182-190)
	1208.3	1208.4	FIEWTRLDK(255-263)
	1464.6	1465.7	MDEEEVEVFLPK(264-275)
	1503.8	1506.7	GTTASQMAQALALDK(47-61)
	1934.2	1936.2	LGMTDAFGGRADFSGMSSK(291-309)
	1953.7	1955.2	TGTQYLLRTANRLFGDK(84-100)
	2250.2	2248.4	CSGNGGGDVHQGFQSLLTEVNK(62-83)
	2467.3	2467.8	EVLSPGTVNSDTSLVLVNAIYFK(150-172)
	3340.9	3342.6	FYEAELEELDFQGATEESRQHINTWVAK(115-142)
	3736.7	3736.1	GTTASQMAQALALDKCSGNGGGDVHQGFQSLLTEVK(47-83)

The 65- and 41-kDa fragments (see Figure 3-2-3) were analyzed.

[1] The peptides of 41K-53, 41K-80, and 65K-96 were directly determined by N-terminal sequencing.

[2] Digested fragments of 65-kDa complex were subjected to mass spectroscopy analysis directly.

[3] The number of SPI3 amino acid sequence in Figure 3-2-4 (parenthesis)

[4] Metionine is oxidized.

N.D.: not detected.

The above molecular mass predicted 57% of SPI3 amino acid sequence.

```
ctcatctcttctctgcttgctaccagtccggaaatcgagaatctaggagaatctagggct
caccatcatggatcctctacaggaagcaaatggcacctttgccttaaatcttttgaaaat
          M  D  P  L  Q  E  A  N  G  T  F  A  L  N  L  L  K  I   18
actgggtgaagacagctcaaaaaatgtatttttgtcacccatgagcatatcctcagccct
       L  G  E  D  S  S  K  N  V  F  L  S  P  M  S  I  S  S  A  L   38
ggctatggtcttcatgggggcaaaaggaaccactgctagccagatggctcaggcacttgc
    A  M  V  F  M  G  A  K  G  T  T  A  S  Q  M  A  Q  A  L  A   58
tttggataaatgcagcggcaatggaggtggagatgtccaccagggcttccagtcccttct
    L  D  K  C  S  G  N  G  G  G  D  V  H  Q  G  F  Q  S  L  L   78
caccgaagtgaacaaaactggcacacagtacttgctcagaacagccaacaggctcttcgg
    T  E  V  N  K  T  G  T  Q  Y  L  L  R  T  A  N  R  L  F  G   98
ggataagacttgtgatcttttagcgtcttttaaagattcctgcctcaagttctatgaagc
    D  K  T  C  D  L  L  A  S  F  K  D  S  C  L  K  F  Y  E  A  118
agagttggaagagctggactttcagggtgctacagaggagtcccgacagcacatcaacac
    E  L  E  E  L  D  F  Q  G  A  T  E  E  S  R  Q  H  I  N  T  138
ctgggtagccaaaaagacagaagataaaatcaaagaggtgctgtctccaggtacagtgaa
    W  V  A  K  K  T  E  D  K  I  K  E  V  L  S  P  G  T  V  N  158
ttctgatacatcgctagtccttgtgaatgccatctacttcaaaggaaactgggagaagca
    S  D  T  S  L  V  L  V  N  A  I  Y  F  K  G  N  W  E  K  Q  178
gtttaacaaagagcataccagggagatgccattcaaagtcagcaagaatgaggagaaacc
    F  N  K  E  H  T  R  E  M  P  F  K  V  S  K  N  E  E  K  P  198
tgtgcaaatgatgtttaagaagtctacctttaagatgacctatattggagagatattcac
    V  Q  M  M  F  K  K  S  T  F  K  M  T  Y  I  G  E  I  F  T  218
taagattctgttgcttccctatgtcagcagtgagctgaacatgatcatcatgcttccaga
    K  I  L  L  L  P  Y  V  S  S  E  L  N  M  I  I  M  L  P  D  238
tgagcacgttgaactgagtacagtggaaaaggaagtaacttacgagaaatttatagagtg
    E  H  V  E  L  S  T  V  E  K  E  V  T  Y  E  K  F  I  E  W  258
gacaaggctggacaagatggacgaagaagaggtagaagtatttctccCCAAAGTTTAAGCT
    T  R  L  D  K  M  D  E  E  E  V  E  V  F  L  P  K  F  K  L  278
GGAGGAGAATTACAACATGAACGATGCCCTCTACAAGTTGGGCATGACTGATGCCTTTGG
    E  E  N  Y  N  M  N  D  A  L  Y  K  L  G  M  T  D  A  F  G  298
CGGCAGGGCAGACTTTTCTGGAATGTCTTCCAAGCAAGGCTTGTTTCTGTCTAAGGTTGT
    G  R  A  D  F  S  G  M  S  S  K  Q  G  L  F  L  S  K  V  V  318
GCATAAGGCCTTTGTGGAGGTTAATGAGGAGGGCACAGAGGCTGCAGCTGCTACAGCTGG
    H  K  A  F  V  E  V  N  E  E  G  T  E  A  A  A  A  T  A  G  338
CATGATGACGGTGAGGTGCATGAGATTCACTCCCCGCTTCTGTGCCGACCACCCCTTCCT
    M  M  T  V  R  C  M  R  F  T  P  R  F  C  A  D  H  P  F  L  358
TTTCTTCATTCACCATGTTAAGACCAATGGAATTCTGTTCTGTGGCCGGTTCTCCTCTCC
    F  F  I  H  H  V  K  T  N  G  I  L  F  C  G  R  F  S  S  P  378
CTGAGCAAAGGGTATTCCTGTCAGtctttgaccctctctccatggtttgctgtaacccaa
gtgaccttatccataagtgcaatggcaattatgaaataaagggctttatggcaccc
```

(continued)

Figure 3-2-4 Nucleotide and Amino Acid Sequence of SPI3 cDNA Nucleotide and amino acid sequences of SPI3 cDNA are shown with small and capital letters, respectively. Blue capital letters show sequences predicted by mass spectroscopy analysis (see Table 3-2-2) and red capital letters are identified by micro-amino-acid sequencing. Bold small letters show the probe sequence used for *in situ* hybridization histochemistry (see Figure 3-2-7).

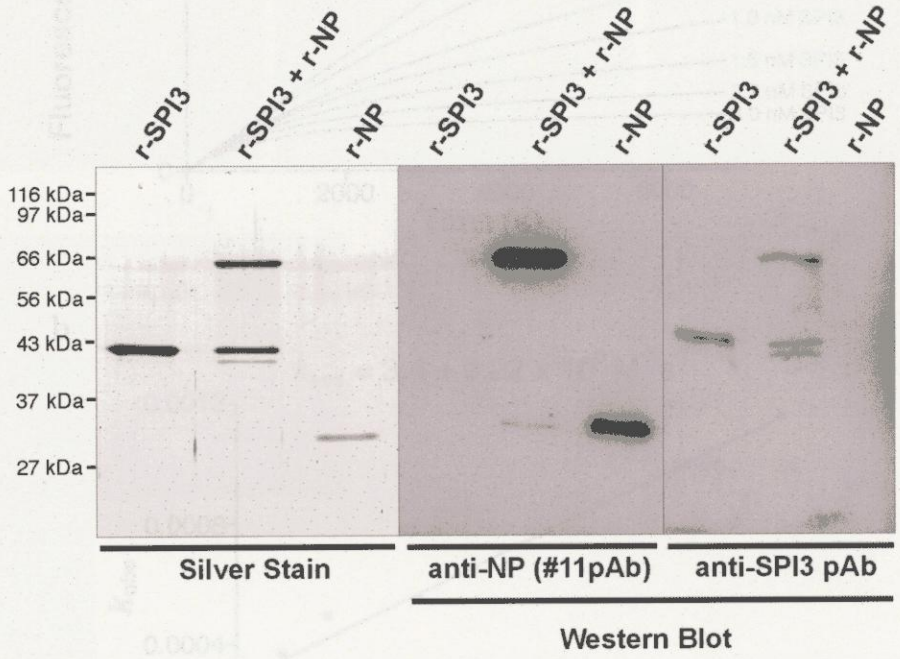

Figure 3-2-5 Detection of SDS-stable Complex of Recombinant Neuropsin and Recombinant SPI3 Activated recombinant neuropsin (baculo) (100 ng) and recombinant SPI3 (200 ng) were mixed and incubated. Three mixed sample sets were subjected to reducing 12.5% SDS-PAGE. One set was silver-stained, and the other two sets were followed by western blot with either anti-neuropsin (#11pAb) or rabbit anti-SPI3 antibody.

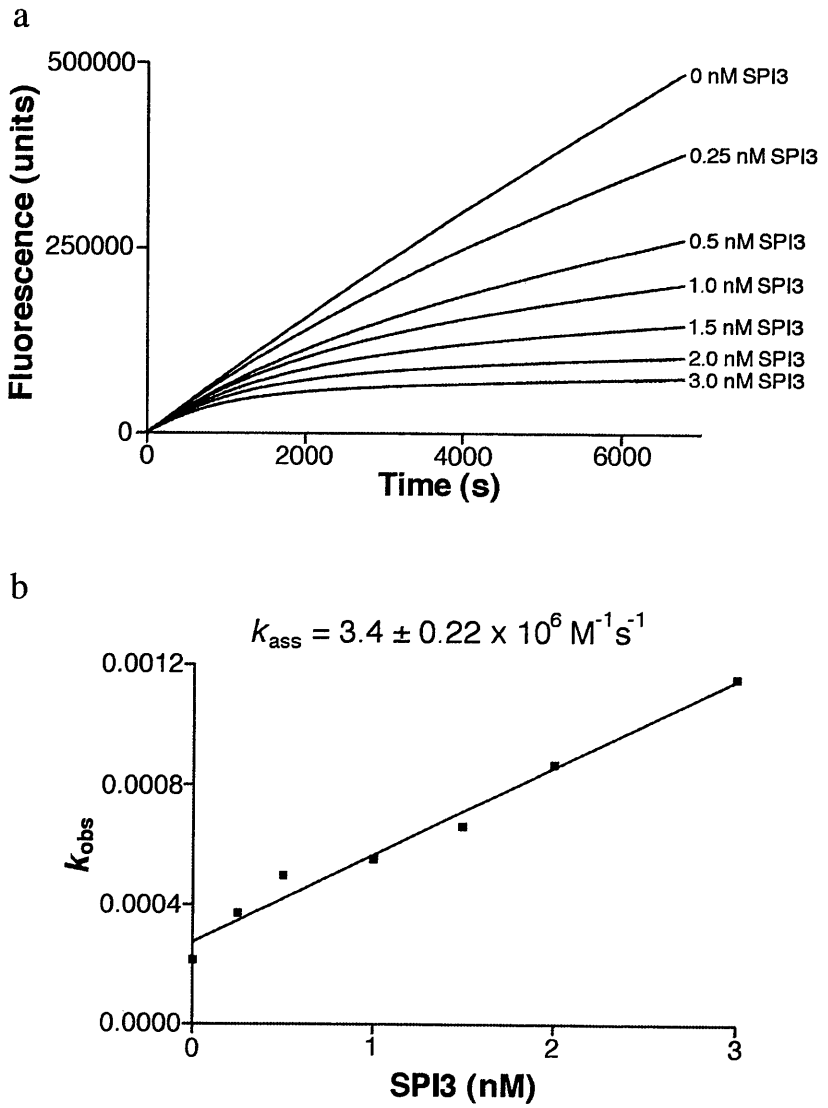

Figure 3-2-6 Kinetic Analysis of Inhibitory Activity of SPI3 against Neuropsin *a*, The residual activities of activated recombinant neuropsin (baculo) were measured using a substrate (Boc-Val-Pro-Arg-MCA) and were plotted against time in the presence of increasing concentrations of SPI3 *b*, A k_{ass} of recombinant SPI3 against activated recombinant neuropsin (baculo) was calculated using observed inhibitory rate (k_{obs}) against different concentrations of recombinant SPI3, indicating a k_{ass} of 3.4 ± 0.22 x 10^6 $M^{-1}s^{-1}$ and a K_i of 0.8 nM.

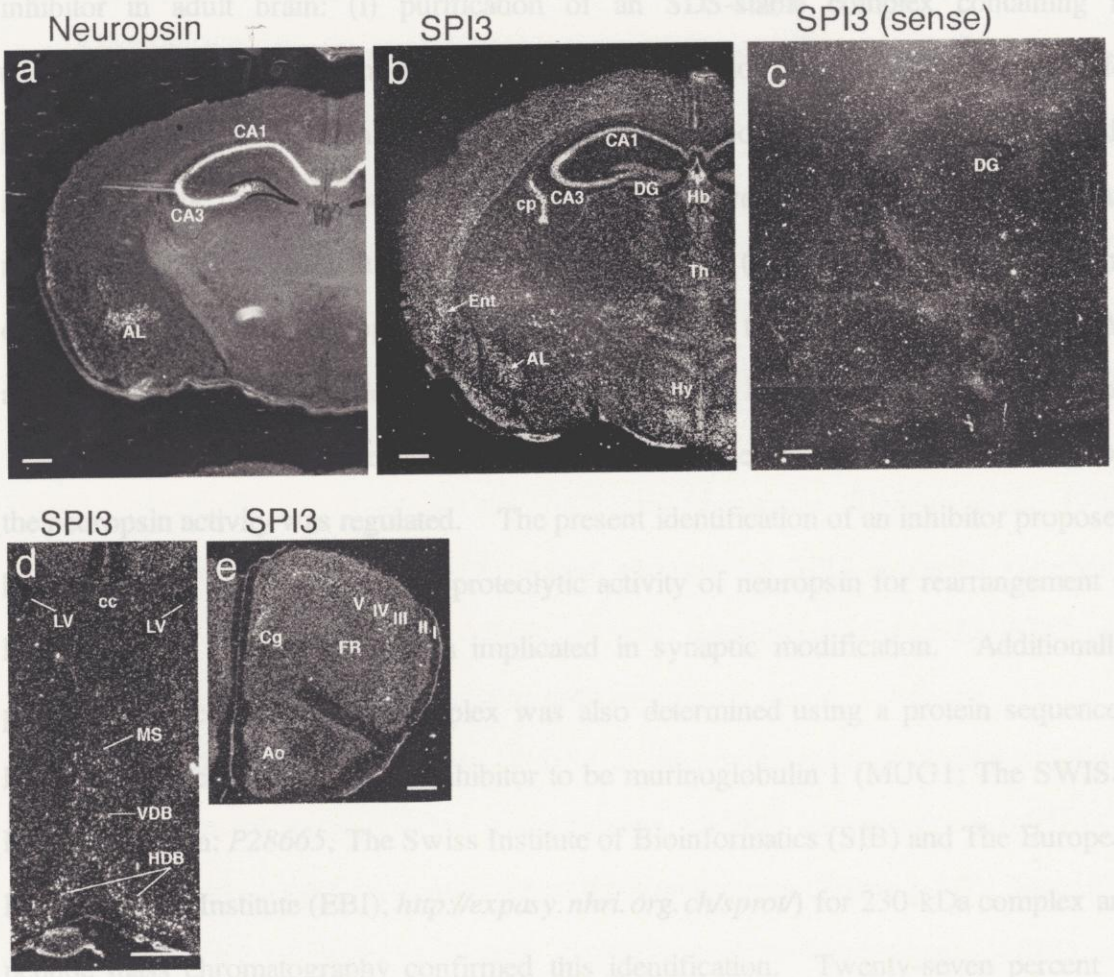

Figure 3-2-7 Distribution of SPI3 and Neuropsin mRNAs in Adult Mouse Brain *In situ* hybridization histochemistry was carried out using 14 μm coronal sections and ^{35}S-labeled SPI3 riboprobes (neuropsin antisense riboprobe for *a*; SPI3 antisense riboprobe for *b*, *d*, and *e*; SPI3 sense riboprobe for *c*). Intense hybridization signals were observed as silver grains under dark-field illumination. Note that no signal was observed with sense probe (*b*). Each white bar shows 500 μm. *I-V*, layers of the frontal cortex; *AL*, amygdaloid complex; *Ao*, anterior olfactory nuclei; *CA1-3*, subfields CA1-3 of Ammon's horn; *cc*, corpus callosum; *Cg*, cingulate cortex, *cp*, choroid plexus in lateral ventricle; *DG*, dentate gyrus; *Ent*, entorhinal cortex; *FR*, frontal cerebral cortex; *Hb*, habenular nucleus; *HDB*, horizontal diagonal band; *Hy*, hypothalamus; *LV*, lateral ventricle; *MS*, medial septal nucleus; *Th*, thalamus; *VDB*, vertical diagonal band.

3-3. DISCUSSION

In the present study, I have obtained evidence that SPI3 is a neuropsin-specific inhibitor in adult brain: (i) purification of an SDS-stable complex containing an endogenous inhibitor within brain extracts, (ii) detection of inhibitory activities for proteolytic effect of recombinant neuropsin, and (iii) co-localization of neuropsin with the inhibitor in the hippocampus. Previous studies have shown that neuropsin has modulated E-LTP dependent on the proteolytic activity (Komai *et al.*, 2000) and that extracellular targets of neuropsin include components of the extracellular matrix (ECM) and the cell adhesion molecule such as fibronectin and L1, but not laminin (Shimizu *et al.*, 1998; Ninomiya *et al.*, in preparation). There has, however, been no evidence of how the neuropsin activity was regulated. The present identification of an inhibitor propose a hypothesis that SPI3 regulates the proteolytic activity of neuropsin for rearrangement of ECM proteins, and as a result, is implicated in synaptic modification. Additionally, peptide sequence of 230-kDa complex was also determined using a protein sequencer. Peptide sequencing identified the inhibitor to be murinoglobulin 1 (MUG1; The SWISS-PROT accession: *P28665*, The Swiss Institute of Bioinformatics (SIB) and The European Bioinformatics Institute (EBI); *http://expasy.nhri.org.ch/sprot/*) for 230-kDa complex and peptide mass chromatography confirmed this identification. Twenty-seven percent of MUG1 was sequenced (data not shown). MUG1 protein also localized in neurons of the hippocampus (data not shown), and MUG1 might regulate the proteolytic activity of neuropsin in the hippocampus.

Previous reports have showed that SPI3 is the mouse homologue of human proteinase inhibitor 6 (PI-6) (Sun *et al.*, 1995a), which possesses inhibitory activities against trypsin, thrombin, and plasmin *in vitro* (Sun *et al.*, 1995b) and against cathepsin G (k_{ass} = 6.8 x 10^6 $M^{-1}s^{-1}$) in monocytes and granulocytes *in vivo* (Scott, *et al.*, 1999). The present study has evaluated that SPI3 was a potent inhibitor specific for neuropsin (k_{ass} = 3.4 x 10^6 $M^{-1}s^{-1}$) in the nervous system. In brain, neuroserpin and protease nexin

1 (PN-1) are proposed to be potent inhibitors of tissue plasminogen activator (tPA; k_{ass} = 1.5 x 10^5 $M^{-1}s^{-1}$) and thrombin (k_{ass} = 6.0 x 10^5 $M^{-1}s^{-1}$), respectively (Scott *et al.*, 1985; Osterwalder *et al.*, 1998). The k_{ass} of SPI3-neuropsin was greater than those of PN-1-thrombin and of neuroserpin-tPA, indicating that inhibition of neuropsin by SPI3 occurs more rapidly and extensively. It is, therefore, suggested that interaction between SPI3 and neuropsin potently occurs *in vivo*.

The SPI3 P1 residue which interacts with neuropsin remains to be identified but is predicted to be Arg^{343}. Previous study has shown that PI-6 and SPI3 both utilize the P1 arginine for interactions with serine proteases possessing trypsin-like activity (Sun *et al.*, 1995a; Coughlin *et al.*, 1993) and that neuropsin was a trypsin-like serine protease showing proteolytic activity against the C-terminus of arginine (Shimizu *et al.*, 1998). Moreover, mutagenesis analysis of neuropsin showed that SPI3 interacted specifically with neuropsin active site (Figure 3-2-2). It was, therefore, predicted that SPI3 used Arg^{353} as the P1 residue for the interaction with neuropsin.

Next, I discuss potential roles of SPI3 in the regulation of neuropsin activity in brain. The present study revealed co-localization of SPI3 and neuropsin mRNAs in pyramidal neurons in the CA1-3 subfields of the hippocampus (Figure 3-2-7), suggesting that SPI3 was also implicated in synaptic modification in the hippocampus. SPI3 was identified as an intracellular protease inhibitor in the lymphocyte system (Scott *et al.*, 1996), while neuropsin is estimated as an extracellular protease. In the present study, SPI3 was detected in a 65-kDa complex with recombinant neuropsin in the 0.15M NaCl-soluble, Triton-soluble, and cytoskeleton-rich fractions (Figure 3-2-1), suggesting that SPI3 both localized in cytosol and associated with the organelle membranes and the cytoskeleton. On the other hand, the endogenous brain SPI3-neuropsin complex was detected only in the Triton-soluble fraction (Figure 3-2-1b), showing that the complex accumulated in this fraction. In addition, pro-type recombinant neuropsin also formed a 65-kDa complex with endogenous SPI3 as well as activated recombinant neuropsin

(Figure 3-2-1a). Previous studies suggested that neuropsin is activated after it is secreted (Momota *et al.*, 1998; Shimizu *et al.*, 1998). Therefore, these results indicate that SPI3 interacts with pro-type neuropsin before it is secreted, or with active-type neuropsin after internalization. It remains to be determined directly when and where SPI3 regulates proteolytic activity of neuropsin.

It has recently been found that human PI-6 was a potent intracellular inhibitor specific for cathepsin G in monocytes and granulocytes (Scott *et al.*, 1999). Cathepsin G is one of the azurophilic granule cytotoxins, which functions in the elimination of bacterial and fungal pathogens, and fibronectin is raised as one of the extracellular targets (McDonald and Kelley, 1980; Blondeau *et al.*, 1993). Additionally, recent findings show that cathepsin G activates a pro-apoptotic protease, caspase-7, suggesting that it has the potential to induce apoptosis intracellularly (Zhou and Salvesen, 1997). Thus, the hypothesis has been proposed that human PI-6 prevented cathepsin G-mediated damage in monocytes and granulocytes. On the other hand, in brain, I propose that SPI3, mouse homologue of human PI-6, prevents neuropsin-mediated damage in neurons. There is evidence that excessive stimulation of glutamate receptors induces a large increase of intracellular Ca^{2+} concentration, leading to neuronal cell death (Choi, 1994; Rothman and Olney, 1995; Segal *et al.*, 2000). I have recently found that glutamate stimulation induces secretion of neuropsin in hippocampal primary cultures (Oka, *et al.*, in preparation). Thus, over-stimulation of the receptors might lead to secretion of excessive neuropsin and failure to control neuropsin by SPI3, resulting in neuronal cell death. Additionally, brain ischemia induced expression of SPI3 mRNA in astrocytes of the hippocampus at 3 days after treatment (Nakaya *et al.*, 1998) and that oxidative stress in mouse brain induced a transient increase of neuropsin mRNA in neurons of the hippocampus at 2 hours after treatment. In these pathological conditions, up-regulation of SPI3 expressions might protect neurons from the excess of internalized active-type neuropsin.

In situ hybridization histochemistry has also showed that several areas in brain expressed either SPI3 or neuropsin mRNAs, not both (Figure 3-2-7). The lateral septal nucleus was labeled with neuropsin but not SPI3 riboprobe. As I purified 65-kDa complex from the hippocampal and cerebral cortical extracts but not from that of the basal forebrain, it remains unclear whether there is other specific inhibitor against neuropsin in the lateral septal nucleus. Several areas were labeled with SPI3 riboprobe but not with neuropsin, which might show that SPI3 interacts with other proteases possessing a substrate specificity resemble in neuropsin.

Finally, the present study has identified natural neuropsin inhibitor, SPI3, in adult brain, suggesting that SPI3 regulates the physiological role mediated by neuropsin in adult brain.

4. LIST OF PUBLICATIONS

1. Kishi, T., Kato, M., Shimizu, T., Kato, K., Matsumoto, K., Yoshida, S., Shiosaka, S., and Hakoshima, T. (1997). Crystallization and preliminary X-ray analysis of neuropsin, a serine protease expressed in the limbic system of mouse brain. *J. Struct. Biol.* **118**, 248-51
2. Kishi, T., Kato, M., Shimizu, T., Kato, K., Matsumoto, K., Yoshida, S., Shiosaka, S., and Hakoshima, T. (1999). Crystal structure of neuropsin, a hippocampal protease involved in kindling epileptogenesis. *J. Biol. Chem.* **274**, 4220-4
3. Takahashi, N., Tsukamoto, Y., Shiosaka, S., Kishi, T., Hakoshima, T., Arata, Y., Yamaguchi, Y., Kato, K., and Shimada, I. (1999). N-glycan structures of murine hippocampus serine protease, neuropsin, produced in Trichoplusia ni cells. *Glycoconj. J.* **16**, 405-14
4. Kato, K., Kishi, T., Kamachi, T., Akisada, M., Oka, T., Midorikawa, R., Takio, K., Dohmae, N., Bird, P., Sun, J., Scott, F., Miyake, Y., Kazuhiko Yamamoto, K., Machida, A., Tanaka, T., Matsumoto, K., Shibata, M., and Shiosaka, S. Serine proteinase inhibitor 3 and murinoglobulin I are potent inhibitors of neuropsin in adult mouse brain. *J. Biol. Chem.*, in press.

5. ACKNOWLEDGMENTS

The present studies have been performed under the direction of professor Toshio Hakoshima (Division of Structural Biology, Nara Institute of Science and Technology).

The author thanks to professor Toshio Hakoshima for his guidance and encouragement throughout these investigations. The author thanks to Dr. M. Kato, Dr. T. Shimizu (Division of Structural Biology) for their guidance of the X-ray crystallography.

The author thanks to professor Sadao Shiosaka (Division of Structural Cell Biology, Nara Institute of Science and Technology) for providing the cells for expression of neuropsin and for supporting of the identification and characterization of SPI3. The author thanks to Dr. K. Kato (Division of Structural Cell Biology) for her guidance of the identification and characterization of SPI3.

The author thanks to Dr. M. Suzuki for data collection at Photon Factory (Tsukuba). The author thanks to Dr. R. Takahashi for analyzing N-glycan of neuropsin (Mitsukan Group Co. Ltd.). The author thanks to Drs. B. Bax (Birkbeck College) and S.E. Won Suh (Seul National University) for providing the coordinates of 7S NGF and soybean trypsin inhibitor-trypsin complex, respectively.

The author thanks to Dr. K. Takio (The Institute for Physical and Chemical Research) for microsequencing of SPI3. The author thanks to Dr. P. Bird (Monash University) for the enzyme assay between neuropsin and SPI3. The author thanks to Dr. T. Tanaka (Osaka University) for sequencing of SPI3 cDNA.

The author thanks to Dr. S. Takayama and Ms. J. Tsukamoto for technical assistance.

The author thanks to all members of Division of Structural Biology and Structural Cell Biology (Nara Institute of Science and Technology) for their kindness and advice.

The present studies were supported by "Research Fellowships of the Japan Society for the Promotion of Science for Young Scientists".

6. APPENDIX - Related World Wide Wave Sites -

The Protein Data Bank (PDB)

provided by The Research Collaboratory for Structural Bioinformatics (RCSB)

http://www.rcsb.org/pdb/

PDB code:
1ABJ: Human α-thrombin complex with D-Phe-Pro-Arg-chloromethylketone
1AO5: Mouse glandular kallikrein-13
1JRS: Bovine pancreatic β-trypsin complex with leupeptin
1NPM: Mouse brain neuropsin
1PPB: Porcine pancreatic β-trypsin complex with soybean trypsin inhibitor
1SGF: Mouse submaxillary gland 7S NGF
2PKA: Porcine pancreatic kallikrein
4PTP: Bovine pancreatic β-trypsin

The Genbank

provided by The National Center for Biotechnology Information (NCBI)

http:// www.ncbi.nlm.nih.gov/ Genbank/GenbankOverview.html

Accession code:
MMU25844: Mouse serine proteinase inhibitor 3 (SPI3)

The Protein Information Resource (PIR)

provided by The National Biomedical Research Foundation (NBRF)

http:// www-nbrf.georgetown.edu/ nbrf/index.html

Accession code:
A57488: Mouse serine proteinase inhibitor 3 (SPI3)

The SWISS-PROT

provided by The Swiss Institute of Bioinformatics (SIB) and The European Bioinformatics Institute (EBI)

http:// expasy.nhri.org.ch/sprot/

Accession code:
P28665: Mouse murinoglobulin 1 (MUG1)

7. REFERENCES

Barrett, A.J., Rawlings, N.D., and Woessner, J.F. ed. (1998) *Introduction: serine peptidases and their clans* In "Handbook of Proteolytic Enzymes" (London: Academic Press), pp. 3-4

Bax, B., Blundell, T.L., Murray-Rust, J., and McDonald, N.Q. (1997) Structure of mouse 7S NGF: a complex of nerve growth factor with four binding proteins. *Structure* **5**, 1275-1285

Blondeau, X., Vidmar, S.L., Emod, I., Pagano, M., Turk, V. and Keil-Dlouha, V. (1993) Generation of matrix-degrading proteolytic system from fibronectin by cathepsins B, G, H and L. *Biol. Chem. Hoppe. Seyler.* **374**, 651-656

Bode, W., Chen, Z., Bartels, K., Kutzbach, C., Schmidt-Kastner, G., and Bartunik, H. (1983) Refined 2 A X-ray crystal structure of porcine pancreatic kallikrein A, a specific trypsin-like serine proteinase. Crystallization, structure determination, crystallographic refinement, structure and its comparison with bovine trypsin. *J. Mol. Biol.* **164**, 237-282

Bode, W., Mayr., I, Baumann, U., Huber, R., Stone, S.R., and Hofsteenge, J. (1989) The refined 1.9 A crystal structure of human alpha-thrombin: interaction with D-Phe-Pro-Arg chloromethylketone and significance of the Tyr-Pro-Pro-Trp insertion segment. *EMBO J.* **8**, 3467-3475

Brünger, A.T. (1992) *Energy Minimization.* In "The X-PLOR version 3.1: A system for X-ray crystallography and NMR" (New Heaven and London: Yale Unversity Press), pp. 125-127

Brünger, A.T. (1992) Free R value: a novel statistical quantity for assessing the accuracy of crystal structures. *Nature* **355**, 472-475

Chambers, J.L. and Stroud, R.M. (1979) The accuracy of refined protein structures: comparison of two independently refined models of bovine trypsin. *Acta Cryst.* B**35**, 1861-1874

Chen, Z.L., Yoshida, S., Kato, K., Momota, Y., Suzuki, J., Tanaka, T., Ito, J., Nishino, H., Aimoto, S., Kiyama, H., and Shiosaka, S. (1995) Expression and activity-dependent changes of a novel limbic-serine protease gene in the hippocampus. *J. Neurosci.* **15**, 5088-5097

Choi, D.W. (1994) Glutamate receptors and the induction of excitotoxic neuronal death. *Prog. Brain Res.* **100**, 47-51

Collaborative Computational Project, Number 4 (1994) The CCP4 suite: programs for protein crystallography. *Acta Cryst.* D**50**, 760-763

Coughlin, P., Sun, J., Cerruti, L., Salem, H.H., and Bird, P. (1993) Cloning and molecular characterization of a human intracellular serine proteinase inhibitor. *Proc. Natl. Acad. Sci. USA* **90**, 9417-9421

Cowtan, K.D. and Main, P. (1996) Phase combination and cross validation in iterated density-modification calculations. *Acta Cryst.* D**52**, 43-48

Crowther, R.A. (1972) *The molecular replacement.* In "Int. Sci. Rev. No. 13", Rossmann, M. G. ed. (Gordon and Breach, New York) pp.173-178

Crowther, R.A. and Blow, D.M. (1967) A method of positioning a known molecule in an unknown crystal structure. *Acta Cryst.* **23**, 544-548

Cudney, R., Patel, S., Weisgraber, K., Newhouse, Y., and McPherson, A. (1994) Screening and optimization strategies for macromolecular crystal growth. *Acta Cryst.* D**50**, 414-4

Gschwend, T.P., Krueger, S.R., Kozlov, S.V., Wolfer, D.P., and Sonderegger, P. (1997) Neurotrypsin, a novel multidomain serine protease expressed in the nervous system. *Mol. Cell Neurosci.* **9**, 207-219

Hedstrom, L., Perona, J.J., and Rutter, W.J. (1994) Converting trypsin to chymotrypsin: residue 172 is a substrate specificity determinant. *Biochemistry* **33**, 8757-8763

Higashi, T. (1990) Auto-indexing of oscillation images. *J. Appl. Cryst.* **23**, 253-257

Hink, W.F. (1970) Established insect cell line from the cabbage looper, *Trichoplusia ni. Nature* **226**, 466-467

Jancarik, J. and Kim, S.H. (1991) Sparse matrix sampling: a screening method for crystallization of proteins. *J. Appl. Cryst.* **24**, 409-411

Jones,T.A., Zou, J.Y., Cowan,S.W. and Kjeldgaad,M. (1991) Improved methods for building protein models in electron density maps and the location of errors in these models. *Acta Cryst.* A**47**, 110-119

Kawasaki, H., Emori, Y., and Suzuki, K. (1990) Production and separation of peptides from proteins stained with Coomassie brilliant blue R-250 after separation by sodium dodecyl sulfate-polyacrylamide gel electrophoresis. *Anal. Biochem.* **191**, 332-336

Komai, S., Matsuyama, T., Matsumoto, K., Kato, K., Kobayashi, M., Imamura, K., Yoshida, S., Ugawa, S., and Shiosaka, S. (2000) Neuropsin regulates an early phase of schaffer-collateral long-term potentiation in the murine hippocampus. *Eur. J. Neurosci.* **12**, 1479-1486

Kurinov, I.V. and Harrison, R.W. (1996) Two crystal structures of the leupeptin-trypsin complex. *Protein Sci.* **5**, 752-758

Laskowski,R.A., MacArthur,M.W., Moss,D.S. and Thornton,J.M. (1993) Programs to check the Stereochemical Quality of Protein Structures. *J. App. Cryst.* **26**, 283

Laemmli, U.K. (1970) Cleavage of structural proteins during the assembly of the head of bacteriophage T4. *Nature* **227**, 680-685

Masaki, T., Tanabe, M., Nakamura, K., and Soejima, M. (1981) Studies on a new proteolytic enzyme from A chromobacter lyticus M497-1. I. Purification and some enzymatic properties. *Biochim. Biophys. Acta* **660**, 44-50

Masutani, C., Kusumoto, R., Yamada, A., Dohmae, N., Yokoi, M., Yuasa, M., Araki, M., Iwai, S., Takio, K., and Hanaoka, F. (1999) The XPV (xeroderma pigmentosum variant) gene encodes human DNA polymerase eta. *Nature* **399**, 700-704

Matthews, B.W. (1968) Solvent content of protein crystals. *J. Mol. Biol.* **33**, 491-497

McDonald, J.A. and Kelley, D.G. (1980) Degradation of fibronectin by human leukocyte elastase. Release of biologically active fragments. *J. Biol. Chem.* **255**, 8848-8858

McPherson, A.Jr. (1976) The growth and preliminary investigation of protein and nucleic acid crystals for X-ray diffraction analysis. *Methods Biochem. Anal.* **23**, 249-345

Mizuguchi, H., Nakagawa, T., Nakanishi, M., Imazu, S., Nakagawa, S., and Mayumi, T. (1996) Efficient gene transfer into mammalian cells using fusogenic liposome. *Biochem. Biophys. Res. Commun.* **218**, 402-407

Momota, Y., Yoshida, S., Ito, J., Shibata, M., Kato, K., Sakurai, K., Matsumoto, K., and Shiosaka, S. (1998) Blockade of neuropsin, a serine protease, ameliorates kindling epilepsy. *Eur. J. Neurosci.* **10** 760-764

Morrison, J.F. and Walsh, C.T. (1988) The behavior and significance of slow-binding enzyme inhibitors. *Adv. Enzymol. Relat. Areas Mol. Biol.* **61**, 201-230

Nakaya, N., Nishibori, M., Wang, Z., Sakiyama, J., and Saeki, K. (1998) The expression and localization of serine proteinase inhibitor PI-6 mRNA in developmental and ischemic mouse brain. *Neurosci Res.* **32**, 221-230

Navaza, J. (1994) AMoRe: an automated package for molecular replacement. *Acta Cryst.* A**50**, 157-163

Nicholls,A. and Honig,B. (1991) A rapid finite difference algorithm, utilising successive over relaxation to solve the Poission-Boltzmann equation. *J. Comput. Chem.* 12, 435-445

Niwa, H., Yamamura, K., and Miyazaki, J. (1991) Efficient selection for high-expression transfectants with a novel eukaryotic vector. *Gene* **108**, 193-199

Okabe, A., Momota, Y., Yoshida, S., Hirata, A., Ito, J., Nishino, H., and Shiosaka, S. (1996) Kindling induces neuropsin mRNA in the mouse brain. *Brain Res.* **728**, 116-120

Osterwalder, T., Cinelli, P., Baici, A., Pennella, A., Krueger, S.R., Schrimpf, S.P., Meins, M., and Sonderegger, P. (1998) The axonally secreted serine proteinase inhibitor, neuroserpin, inhibits plasminogen activators and plasmin but not thrombin. *J. Biol. Chem.* **273**, 2312-2321

Otwinowski, Z. and Minor, W. (1996) Processing of X-ray diffraction data collected in oscillation mode. *Methods Enzymol.* **276**, 307-326

Perona, J.J. and Craik, C.S. (1997) Evolutionary divergence of substrate specificity within the chymotrypsin-like serine protease fold. *J. Biol. Chem.* **272**, 29987-29990

Potempa, J., Korzuš, E., and Travis, J. (1994) The serpin superfamily of proteinase inhibitors: structure, function, and regulation. *J. Biol. Chem.* **269**, 15957-15960

Rossmann, M.G. and Blow, D.M. (1962) The detection of sub-units within the crystallographic asymmetric unit. *Acta Cryst.* **15**, 24-31

Rothman, S.M. and Olney, J.W. (1998) Excitotoxicity and the NMDA receptor--still lethal after eight years. *Trends Neurosci.* **18**, 57-58

Salvesen, G. and Nagase, H. (1989) *Inhibition of protelytic enzymes.* In "Proteolytic enzymes: a practical approarch", Beynon, R.J. and Bond, J.S. ed. (Oxford: IRL Press), pp. 83-104

Scarisbrick, I.A., Towner, M.D., and Isackson, P.J. (1997) Nervous System-Specific Expression of a Novel Serine Protease: Regulation in the Adult Rat Spinal Cord by Excitotoxic Injury. *J. Neurosci.* **17**, 8156-8168

Scott, F.L., Coughlin, P.B., Bird, C., Cerruti, L., Hayman, J.A., and Bird, P. (1996) Proteinase inhibitor 6 cannot be secreted, which suggests it is a new type of cellular serpin. *J. Biol. Chem.* **271**, 1605-1612

Scott, F.L., Hirst, C.E., Sun, J., Bird, C.H., Bottomley, S.P., and Bird, P.I. (1999) The intracellular serpin proteinase inhibitor 6 is expressed in monocytes and granulocytes and is a potent inhibitor of the azurophilic granule protease, cathepsin G. *Blood* **93**, 2089-2097

Scott, R.W., Bergman, B.L., Bajpai, A., Hersh, R.T., Rodriguez, H., Jones, B.N., Barreda, C., Watts, S., and Baker, J.B. (1985) Protease nexin. Properties and a modified purification procedure. *J. Biol. Chem.* **260**, 7029-7034

Segal, I., Korkotian, I., and Murphy, D.D. (2000) Dendritic spine formation and pruning: common cellular mechanisms ? *Trends Neurosci.* **23**, 53-57

Shimizu, C., Yoshida, S., Shibata, M., Kato, K., Momota, Y., Matsumoto, K., Shiosaka, T., Midorikawa, R., Kamachi, T., Kawabe, A., and Shiosaka, S. (1998) Characterization of recombinant and brain neuropsin, a plasticity-related serine protease. *J. Biol. Chem.* **273**, 11189-11196

Shiosaka, S. and Yoshida, S. (2000) Synaptic microenvironments - structural plasticity, adhesion molecules, proteases and their inhibitors. *Neurosci. Res.* **237**, 85-89

Song, H.K. and Suh, S.W. (1998) Kunitz-type soybean trypsin inhibitor revisited: refined structure of its complex with porcine trypsin reveals an insight into the interaction between a homologous inhibitor from Erythrina caffra and tissue-type plasminogen activator. *J. Mol. Biol.* **275**, 347-363

Sun, J., Coughlin, P., Salem, H.H., and Bird, P. (1995a) Production and characterization of recombinant human proteinase inhibitor 6 expressed in *Pichia pastoris*. *Biochim. Biophys. Acta* **1252**, 28-34

Sun, J., Rose, J.B., and Bird, P. (1995b) Gene structure, chromosomal localization, and expression of the murine homologue of human proteinase inhibitor 6 (PI-6) suggests divergence of PI-6 from the ovalbumin serpins. J. *Biol. Chem.* **270**, 16089-16096

Timm, D.E. (1997) The crystal structure of the mouse glandular kallikrein-13 (prorenin converting enzyme). *Protein Sci.* **6**, 1418-1425

Tohyama, Y., Yanagi, S., Sada, K., and Yamamura, H. (1994) Translocation of p72syk to the cytoskeleton in thrombin-stimulated platelets. *J. Biol. Chem.* **269**, 32796-32799

Yamashiro, K., Tsuruoka, N., Kodama, S., Tsujimoto, M., Yamamura, Y., Tanaka, T., Nakazato, H., and Yamaguchi, N. (1997) Molecular cloning of a novel trypsin-like serine protease (neurosin) preferentially expressed in brain. *Biochim. Biophys. Acta* **1350**,

Zhou, Q. and Salvesen, G.S. (1997) Activation of pro-caspase-7 by serine proteases includes a non-canonical specificity. *Biochem. J.* **324**, 361-364